

SURVIVAL OF LIGNIN-DERIVED STRUCTURAL UNITS IN ANCIENT COALIFIED WOOD SAMPLES

Patrick G. Hatcher and Harry E. Lerch, III

U. S. Geological Survey, Reston, VA 22092

ABSTRACT

Analysis of five Cretaceous-age and one Carboniferous-age fossil wood samples of lignite rank by pyrolysis-gas chromatography-mass spectrometry has revealed the presence of lignin-derived compounds such as phenols and methoxyphenols. In Cretaceous lignitic wood, the various methoxyphenols were of the same suite as those produced from pyrolysis of modern lignin and degraded wood. Indications are that the lignin structural units of Cretaceous lignitic wood samples are preserved to varying degrees. In Carboniferous lignitic wood only traces of methoxyphenols were detected, but phenols were abundant. This is the first indication that lignin-derived methoxyphenols can survive in geological materials as old as the Carboniferous.

INTRODUCTION

Lignin is a major biochemical component of woody tissue; however, it rarely survives early stages of coalification. Biochemical and chemical alteration during burial limit the extent to which lignin biomarkers can be preserved and recognized in the geologic record. Lignin-derived compounds have been observed in pyrolysis products of low rank coals and associated woody tissue[1-5]. Mycke and Michaelis[6] isolated lignin-derived methoxyphenols from a Miocene coal by catalytic hydrogenolysis. Sigleo[7,8] reported the presence of phenolic compounds derived from alteration of lignin in pyrolysis products of silicified woody tissue as old as Triassic age. However, no trace of methoxyphenols, that would clearly relate back to lignin structures, could be identified in Sigleo's samples. Hayatsu *et al.*[9] similarly reported the presence of lignin-derived products from copper-oxide oxidation of several coal samples. They, too, were unable to identify methoxylated phenols in their products. Recently, Nip *et al.*[2] subjected two lignite samples, one of Paleocene age and the other of Eocene age, to Curie-point pyrolysis-mass spectrometry. The data indicated only traces of methoxyphenols. They were puzzled by the low abundance of phenols in general, because the petrographic data indicated large amounts of huminite derived from woody tissue.

The most definitive identification of lignin-derived pyrolysis products in coalified wood samples as old as Paleocene age was reported in a study of coalified wood by Stout *et al.*[4]. They identified numerous lignin-derived methoxyphenols in angiospermous and gymnospermous wood samples from various lignites by Curie-point pyrolysis-gas chromatography-mass spectrometry. In a study of lignitic gymnospermous wood samples of Cretaceous and younger ages by analytical pyrolysis[5], we reported the presence of methoxyphenols in the pyrolyzates. Many of these methoxyphenols had associated propenyl side chains indicative of the presence of well-preserved lignin residues.

In an attempt to delineate the degree of preservation of lignin in coal, we examined numerous coalified wood samples ranging from Carboniferous to Holocene age. The samples were initially screened by solid-state C-13 nuclear magnetic resonance to detect the possible presence of methoxyl carbon. Once such carbons were detected, the samples were subjected to analytical pyrolysis to determine the content of methoxyphenols which would provide an indication of the state of preservation of the lignin-derived structural units. We report here on the

identification of lignin-derived methoxyphenols in the coalified wood samples selected for analytical pyrolysis.

SAMPLES AND METHODS

Samples of coalified wood (xylem) were obtained from Carboniferous and younger strata in various locales. A sample of coalified wood was collected by D. Gottfried (U. S. Geological Survey) from the Magothy Formation (Upper Cretaceous) at the C&O canal near Bethel, Maryland. Byrd Stadium lignitic wood was collected by the late I. A. Breger (U. S. Geological Survey) from an excavation for Byrd Stadium on the campus of the University of Maryland. The coalified logs at this site were buried in an upright position in sediments of the Potomac Group (Lower Cretaceous). Wayne Newell (U. S. Geological Survey) graciously provided a sample (Stafford lignite) of coalified wood buried in sediments of the Potomac Group (Lower Cretaceous) near Stafford, Virginia. Another sample was obtained by Roger Thomas (U. S. Geological Survey) from the Patapsco Formation of the Potomac Group (Lower Cretaceous) near the intersection of I-95 and I-695 in Landsdowne, Maryland. Another sample (Long Island lignite) was obtained by Byron Stone (U. S. Geological Survey) from probable Pleistocene clay in the Nassau Brick Co. clay pit on Long Island, New York; the sample probably was reworked from the Magothy Formation (Upper Cretaceous). Finally, a sample of coalified wood was obtained from the collection of the late I. A. Breger, and this sample was from the Carboniferous lignite deposits of the Moscow Basin, USSR, Kurovskaya mine No. 1. All samples were essentially of lignite rank as partially demonstrated by the elemental data in Table 1.

Table 1. Elemental compositions (dry mineral-matter free) for coalified wood samples.

Lignite Sample	Wood type	%C	%H	%N	%O
Stafford	G	74.9	4.98	0.58	18.9
Long Island	NA	61.1	4.57	0.33	34.0
Patapsco	G	65.7	5.00	0.27	29.3
Byrd Stadium	G	59.2	3.17	0.21	36.3
Magothy	G	72.2	4.43	0.21	22.0
Moscow Basin	NA	NA	NA	NA	NA

G- gymnospermous wood

NA-data not available

Pyrolysis-gas chromatography-mass spectrometry was performed on a Dupont 490B gas chromatograph-mass spectrometer system interfaced with a Technivent Vector 1 data system and a Chemical Data Systems model 120 pyroprobe. Pyrolysis-gas chromatography was performed with a Perkin-Elmer Sigma 2B gas chromatograph interfaced to the pyroprobe. The fused silica column was a 50% phenylmethylsilicone phase available from Hewlett-Packard. Operating conditions and specific methodologies have been given in a previous report[5].

The presence of lignin structural units was confirmed by pyrolysis-gas chromatography-mass spectrometry using comparisons of mass spectra to library spectra, to spectra of authentic standards, and to published mass spectra of lignin phenols[10].

RESULTS AND DISCUSSION

Pyrolysis of Cretaceous lignitic xylem has been shown in a previous report[5] to yield abundant quantities of methoxyphenols derived from the lignin residues preserved in the lignitic woods. The state of preservation can be determined by the abundance of methoxyphenols relative to other altered lignin byproducts such as the phenols and catechols. Figure 1 shows the pyrograms for two samples representative of most of the Cretaceous age lignitic wood in which the state of preservation of lignin varies widely. Peaks for guaiacol, 4-methylguaiacol, 4-vinylguaiacol, 4-ethylguaiacol, eugenol, *cis*- and *trans*-isoeugenol, vanillin, and acetoguaiaconone are clearly the major products in the Long Island lignite, the one representative of lignitic wood samples in which lignin-derived structures are believed to be the least altered. These specific methoxyphenols are clearly derived from lignin precursors or partially altered lignin that has survived in the lignitic wood samples. Extensively altered lignin products such as phenol, the cresol isomers, catechol isomers, and the alkylphenols are also major components of the pyrogram, but they are subordinate to the methoxyphenols in the Long Island lignite. In the Magothy lignite, the phenols and cresols are dominant over the methoxyphenols, indicating that the lignin residues in this sample are significantly more altered than in the Long Island lignite. The degree of lignin preservation varies widely among the lignitic wood samples. In wood samples of subbituminous rank, methoxyphenols have not been detected; the dominant pyrolysis products are phenols and cresols[5].

Analytical pyrolysis of gymnospermous lignin that is minimally altered has been shown to yield the same products as those mentioned above for the least coalified wood samples, although the relative peak intensities may be different[10,12,13]. Figure 2 shows a pyrogram for a gymnospermous log (Atlantic White Cedar, *Chamaecyparis thyoides*) buried in peat from the Great Dismal Swamp, Virginia. Previous studies have shown that most of the cellulosic components of this sample have been degraded microbiologically, leaving lignin relatively unaltered[14]. The pyrogram confirms this by showing a product distribution that is typical of lignin[12], although the broad peak for levoglucosan indicates a small amount of cellulosic material is present. The four largest peaks are for 4-methylguaiacol, 4-vinylguaiacol, guaiacol, and *trans*-isoeugenol in decreasing order of intensity. The relatively high abundance of methoxyphenols having the 3-carbon side chain (eugenol, the isoeugenols, coniferaldehyde, and guaiacylpropan-2-one) and the low abundance of methylvanillate, vanilloyl methyl ketone, and vanillic acid is evidence that the lignin is not altered extensively[12]. Also, the presence of only trace levels of phenols, cresols, and catechols in the buried log is evidence for unaltered lignin.

The lesser quantities of methoxyphenols having the 3-carbon side chain, relative to the other methoxyphenols, in the Cretaceous lignitic wood samples, compared to the modern buried cedar, are an indication that the lignin in the Cretaceous samples has been altered significantly. For example, the ratio of peak intensities, for guaiacol/*trans*-isoeugenol, is 1.3 for the modern buried cedar, whereas the Cretaceous lignitic samples have values that range from 4.8 to 11. This more than five-fold increase in the ratio is indicative of the fact that the lignin molecules in the lignitic woods are altered at the side-chain sites.

Although the lignin-derived methoxyphenols are important components of the pyrolysis of Cretaceous lignitic wood samples, phenols, catechols, and methylated phenols are equally important. The ratio of phenols+catechols to methoxyphenols ranges from 1.0 to 4.9 in the lignitic woods. In the buried cedar, this ratio is 0.10, indicative of the fact that lignin-derived methoxyphenols are the principal constituents and the phenols and catechols, the products of altered lignin, are subordinate. Sigleo[7] suggested that phenols, cresols, and catechols in pyrolysis products of 200-million-year-old petrified wood are derived from altered lignin. We support this conclusion, primarily because lignin is the most likely source of phenols in the lignitic

woods and because of the abundance of lignin-derived methoxyphenols which are co-produced during pyrolysis.

The pyrolysis data for the lignitic wood from the Moscow Basin are shown in Figure 3. The major pyrolysis products are alkylbenzenes, but phenol and alkylphenols comprise major peaks in the pyrogram (Figure 3a). Only a trace of methoxyphenol (Figure 3b) and methylmethoxyphenol (Figure 3c) could be detected in the sample. However, the trace presence of these two methoxyphenols is clear indication that lignin-like material was present in the wood and that only a trace of it remains, albeit in a highly altered form. Thus, the presence of the methoxyphenols in pyrolysis products indicates that lignin-derived components have survived for approximately 300 million years. It is interesting that three isomers of methoxyphenol can be detected in the selected ion trace of m/z 124 (Figure 3b). That these specific peaks were indeed methoxyphenols was determined by retention times and by examination of the fragment ions at m/z 109 and 81. Similarly, the verification of the presence of methylmethoxyphenol was made by retention time and by examination of fragment ions at m/z 123 and 95. Only one isomer of methylmethoxyphenol was detected (Figure 3c) and its retention time on the column corresponds to that of 4-methylguaiacol. Direct comparison of mass spectra to library spectra of authentic methoxyphenols was not possible due to the trace quantities and the complexity of the pyrolysis mixture in the retention-time windows for elution of the methoxyphenols.

Phenol, the cresol isomers, and the dimethylphenols, major pyrolysis products in the Moscow wood sample, are probably also derived from lignin precursors that have been altered through coalification reactions. Hatcher *et al.*[5] have shown that an increase is observed in the relative proportion of phenols and cresols as rank of coalified wood samples increases to subbituminous coal. Comparing the pyrolysis products from the Moscow wood to other coalified wood samples of Hatcher *et al.*[5] allows us to deduce that the Moscow wood is more similar to coalified wood of subbituminous rank than it is of coalified wood of lignite rank, assuming that its lignin was originally similar to lignin in Cretaceous or younger woods.

CONCLUSIONS

The analysis of lignitic woods by analytical pyrolysis has shown that lignin structural units can be preserved as biomarkers in samples as old as Carboniferous age, or approximately 300 million years. At least half or more of the pyrolysis products in lignitic wood of Cretaceous age are methoxyphenols characteristic of lignin. The product distributions in these Cretaceous samples indicate that the lignin is mainly altered in the side chains. Phenols, cresols, catechols, and other methylated phenols account for the remainder of the pyrolysis products. It is likely that these products are also derived from lignin, especially lignin that has been altered by coalification reactions.

ACKNOWLEDGMENTS

We thank our colleagues at the U. S. Geological Survey, Roger Thomas, David Gottfried, Byron Stone, and Wayne Newell, for providing samples for this study.

REFERENCES

1. Philp, R. P., Russell, N. J., Gilbert, T. D., and Friedrich, J. M., *J. Anal. Appl. Pyrol.*, **4**, 143-161, (1982).
2. Nip, M., de Leeuw, J. W., Schenck, P. A., Meuzelaar, H. L. C., Stout, S. A., Given, P. H., and Boon, J. J., *J. Anal. Appl. Pyrol.*, **8**, 221-239, (1985).

3. Chaffee, A. L., Johns, R. B., Baerken, N. J., de Leeuw, J. W., Schenck, P. P., and Boon, J. J., *Org. Geochem.*, **6**, 409-416, (1984).
4. Stout, S. A., Boon, J. J., and Spackman, W., *Geochim. Cosmochim. Acta*, **52**, 405-414, (1988).
5. Hatcher, P. G., Lerch, H. E., III, Kotra, R. K., and Verheyen, T. V., *Fuel*, **67**, 1069-1075, (1988).
6. Mycke, B., and Michaelis, W., *Naturwissenschaften*, **73**, 731-734, (1986).
7. Sigleo, A. C., *Geochim. Cosmochim. Acta*, **42**, 1397-1405, (1978).
8. Sigleo, A. C., *Science*, **200**, 1054-1056, (1978).
9. Hayatsu, R., Winans, R. E., McBeth, R. L., Scott, R. G., Moore, L. P., and Studier, N. H., *Nature*, **278**, 41-43, (1979).
10. Obst, J. R., *J. Wood Chem. Technol.*, **3**, 377-397, (1983).
11. van de Meent, D., Brown, S. C., Philp, R. P., and Simoneit, B. R. T., *Geochim. Cosmochim. Acta*, **44**, 999-1013, (1980).
12. Saiz-Jimenez, C., and de Leeuw, J. W., *Org. Geochem.*, **6**, 417-422, (1984).
13. Saiz-Jimenez, C., Boon, J. J., Hedges, J. I., Hessels, J. K. C., and de Leeuw, J. J., *J. Anal. Appl. Pyrol.*, **11**, 437-450, (1987).
14. Hatcher, P. G., Romankiw, L. A., and Evans, J. R., *Proc. 1985 Int. Conf. Coal Science*, 616-617, (1985).

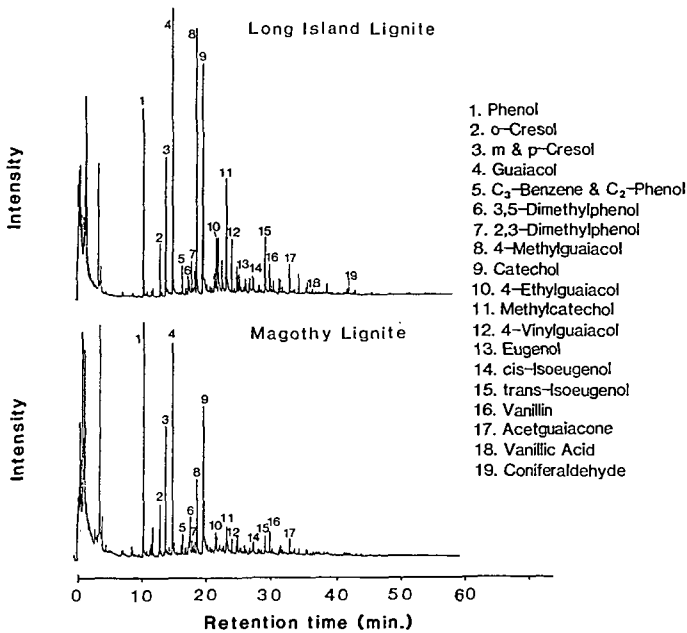


Figure 1. Pyrolysis-gas chromatography of two Cretaceous lignitic wood samples. Numbers above the peaks refer to identified pyrolysis products listed to the right.

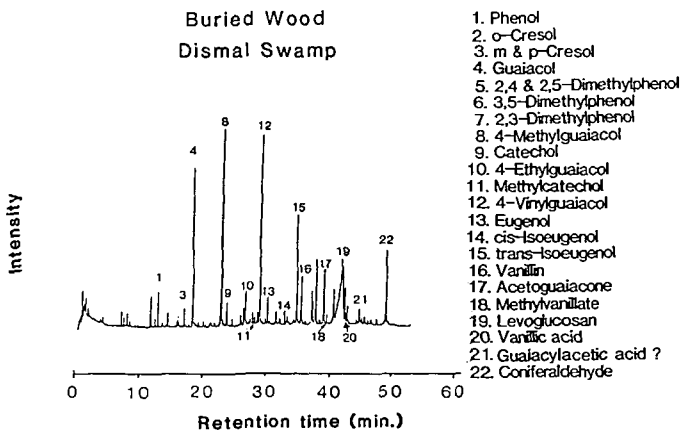


Figure 2. Pyrolysis-gas chromatography of Atlantic White Cedar from the Dismal Swamp, VA. Numbers above the peaks refer to identified pyrolysis products listed to the right.

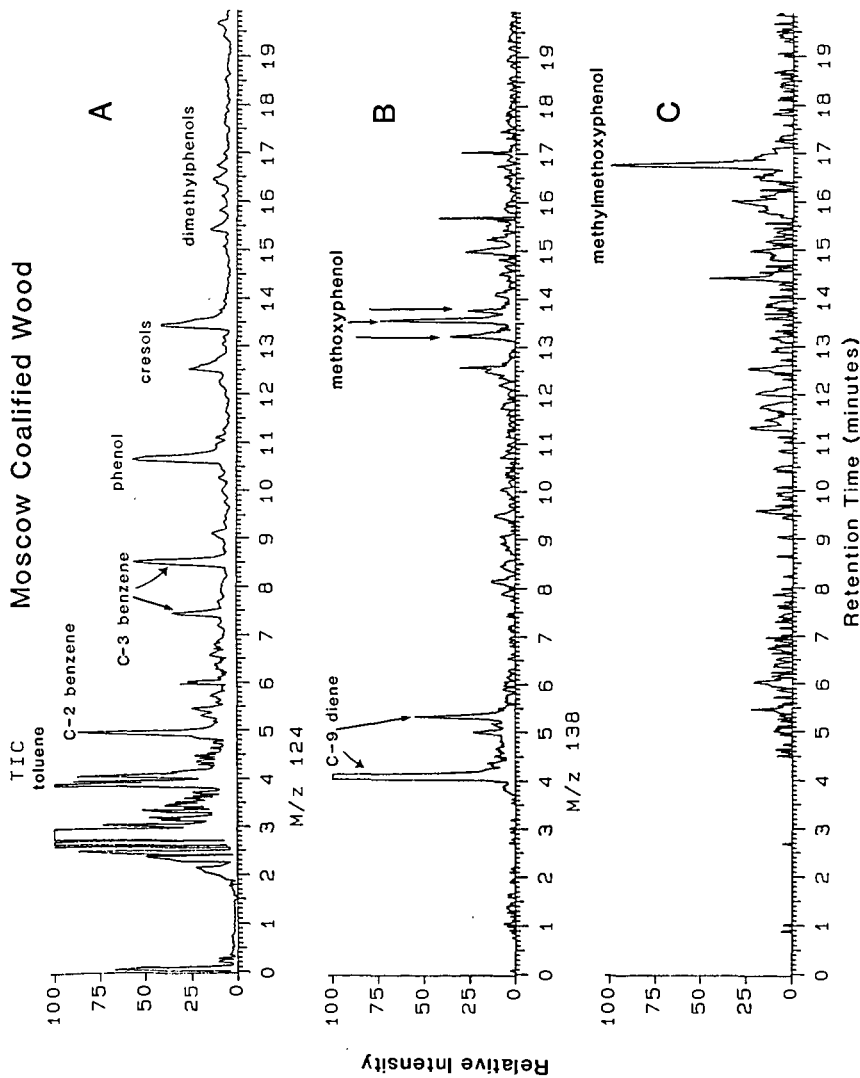


Figure 3. Pyrolysis-gas chromatography-mass spectrometry of the coalified wood from the Moscow Basin lignite. Trace A represents the total ion chromatogram (TIC), B represents the mass chromatogram for m/z 124, and C represents the mass chromatogram for m/z 138. Peak assignments are listed.

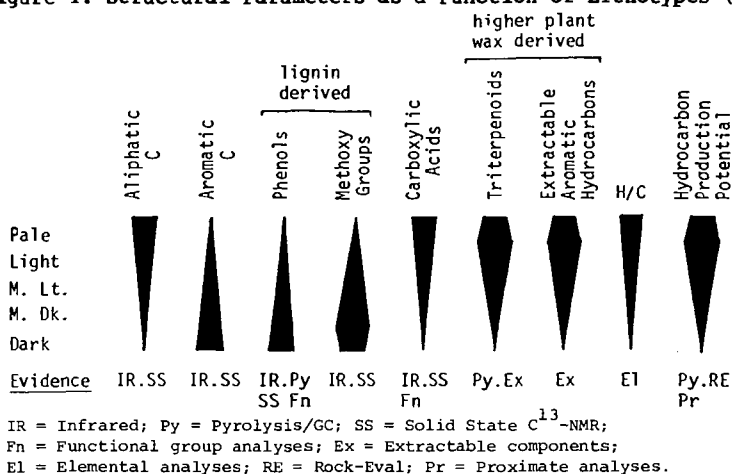
REACTIVITY AND REACTIONS OF SOME AUSTRALIAN BROWN COALS

R.B. Johns and A.G. Pandolfo

Department of Organic Chemistry, University of Melbourne,
Parkville, Victoria, Australia 3052.

The brown coal seams situated in the Latrobe Valley, Victoria, Australia are known to derive predominantly from a higher plant input (1) and represent approximately 25% of the world's supply of brown coal (2). The coals occur in five major lithotypes whose chemical composition vary from one another as illustrated in Figure 1.

Figure 1. Structural Parameters as a Function of Lithotypes (3)



The high water content of Victorian brown coals at approximately 60% is characteristic of these coals but its removal has proved economically disadvantageous. It has recently proved possible, however, to reduce the water content to approximately 10% in a process of densification (4) which is under patent protection (5). The densified brown coal (DBC) produced compares favourably in its Net Wet Specific Energy with a black coal and retains all the other gross characteristics of the raw brown coal.

Densification can also be regarded as a dewatering process. The scheme of production of a DBC is shown in Figure 2 (4) whilst Figure 3 illustrates the loss of moisture with time at ambient temperature and relative humidity. This release of water from the pores of the coal whilst initiated by the attritioning procedure is accompanied by chemical cross-linking reactions and the main thrust of this paper is to explore the chemical aspects of densification.

Table 1. Comparison of Black and Brown Coals with Densified Brown Coal from the Morwell (Vic) Seam.

	Brown coal Morwell, Vic.	Black coal Tarong, Qld.	Densified brown coal
Moisture	59% wb	5.2% adb	15.9% adb
Volatile matter	49.2% db	29.7% db	48.9% db
Fixed carbon	48.8% db	40.9% db	49.1% db
Ash	2.4% db	29.4% db	2.4% db
Total sulphur	0.3% db	0.42% db	0.3% db
GSE	27.2 MJ/kg daf	31.98 MJ/kg daf	27.2 MJ/kg daf
NWSE	8.4 MJ/kg	21.3 MJ/kg adb	22.0 MJ/kg adb
Bulk density	1130 kg/m ³		1200-1700 kg/m ³

wb - wet basis. adb - air dry basis. db - dry basis. daf - dry ash free. GSE - gross specific energy on a dry ash free basis. NWSE - net wet specific energy.

Victorian brown coals are not only chemically complex in components but are physically porous. Kneading will reduce the particle size of the coal and liberate water from the pore structure forming a slurry or paste. Figure 4 illustrates the effects of kneading on the changes in diameter of 10mm pellets on drying. The shrinkage observed is a consequence of loss of water content but also of the development of considerable strength in the pellets as Figure 5 illustrates. Morwell DBC pellets can sustain a load of 280kg at a crush strength of 35MPa. There is a marked difference between the crush strengths developed in DBC from Loy Yang and Morwell coals (Fig. 5) although particle size is the same for both coals. This difference is reflected also in porosities after densification (37% volume porosity for Loy Yang coal versus 14.6% for Morwell) which appear to be the inverse of crush strengths (5.7 for Loy Yang versus 18.5 MPa for Morwell). Pellet shrinkage and the development of crush strength with time can be interpreted as chemical cross-linking reactions drawing microdomains together and in the process excluding water and densifying. Strong pellets may develop cracks on the surface and the crush strengths measured reflect the point of greatest weakness. The shattered fragments retain their strength however.

In seeking to explain these physical changes in terms of chemical reactions it is unlikely that only one class of reactions is involved; rather a range of chemical interactions must be considered. It is known that Victorian brown coals do contain stable free radicals and that as the coal particles are brought closer together by the physical kneading, radical couplings could occur which include cross-linking reactions. We have often noted that a small crush strength maximum develops in the early stages of attritioning which probably occurs as a result of this type of bond formation. Additional forms of bonding would involve ionic reactions, the most likely centres of reaction being carboxyl groups, phenols and activated aromatic systems. The strong pH control of development of crush strength suggests that ionic reactions are the probable cross-linking reactions. Figures 3 - 5 show how densification is coal dependent, but Figure 1 illustrates how compositional differences will also be lithotype-dependent so

that the averaged reactivities of ROM coals integrate several variables.

A dominating parameter in the control of crush strength (σ_c) of DBC pellets is the pH of the raw coal (Figure 6). Coals have a natural pH which may vary depending upon storage time and exposure to air. The more acidic the coal, the smaller the crush strength of the DBC. However, basic additives can raise the crush strengths as illustrated for NaHCO_3 as an additive to Loy Yang coal (Figure 6). Loy Yang is a naturally acidic coal (pH 3.2) but shows a dramatic change in σ_c with increase of pH. NaOH, a strong base, when used as an additive gives a DBC showing a maximum σ_c at approximately pH 6. This is close to the pH (5.3) determined for ROM Morwell coal and thus explains why a strong base additive does not usefully improve its performance during densification.

Clearly, (i) the O-/OH and COO-/COOH ratios in the brown coals, (ii) the absolute abundances of these functional groups, and (iii) their sensitivity to pH are major controlling factors in determining crush strength. In turn these oxygen functional groups can be expected to interact by substituting in activated aromatic systems in the coal. Again, pH will be important in facilitating such interactions. The molecular complexity of the likely reactions will mean that at best a range only of reactions and reactivities will be observed. Given that oxygen functionalities can be expected to play a significant role in densification, one probe would be to sequester acidic hydroxyl groups and observe the effect on crush strengths on densification.

Methylation of brown coals using tetrabutylammonium hydroxide/methyliodide as the methylating agent has an advantage that it swells the coal and utilises the water already inherent in the coal. Methylation affects densification in two ways: first, the DBC formed is weak (Table 2). By removing many of the acidic OH groups through methylation they are unable to form new chemical bonds, although some activation of the attached ring systems by methoxy substituents will be retained. The low σ_c values recorded can be interpreted as a consequence of the inhibition of the intermolecular bonding between particle surfaces. The second observation was that the paste produced on kneading was very moist indeed and consequently generates very little plastic strength. Methylated coal had lost most of its capacity to hold water in its pores presumably because of the reduction in H-bonds to oxygen groups in pore wall surfaces.

The decrease in crush strength maximum of the DBC (Figure 5) on extended drying we believe to be real and probably results from decreased H-bonding. This observation as well as those cited above are consistent with our hypothesis that cross-linking chemical reactions involving acidic hydroxyls and activated aromatised ring systems are involved in the development of microdomains between coal particles. They are also primarily involved in the development of the macrodomain strength in addition to compaction as a physical process and H-bonding by the residual water molecules, some of which will occupy pore space in the macrodomains.

Victorian brown coals can be fractionated into Solvent

Soluble Extracts (SSE), Humic Acids (HA) and a Kerogen (K) residue (6). These are lithotype dependent in concentration hence ROM coals will be variable also in the relative composition of functional groups reactive in densification. SSE have high H/C ratios (7) but do contain some acidic components. These latter could be involved in domain development but on first principles HA and K fractions may be expected to provide good substrates for cross-linking. Indeed humic acids have been implicated in the formation of Solar Dried Coal (8). In our tests neither HA or K additives enhanced the crush strengths derived from LY DBC. The complication of pH, as yet unresolved, clouds the interpretation however, since HA additives are acidic in nature and lower the pH of the raw coal feed. Low pH coals do not develop a significant crush strength in general, nor in the particular, as shown in Table 2 for Loy Yang coal.

Table 2. Effects of Kerogen and Humic Acid Additives on Densification.

Coal	Additive	pH	Crush Strength (MPa)
Loy Yang ROM	None	3.9	6.8
	25% Kerogen	4.3	8.3
	NaHCO ₃	4.9	16.1
	20% Humic acid	3.5	5.8
	20% HA + NaOH	5.9	18.1

Densification offers an advantage in that it readily allows the formation of a moulded coal but importantly the gross characteristics of DBC are still those of the ROM coal (Table 2). Figure 7 exemplifies this well in that the pyrograms for Loy Yang ROM and DBC are very similar. Thermal desorption of brown coal at 350°C releases primarily triterpenoid components which are virtually lacking in the 600°C pyrogram. Thermal desorption of DBC with a base additive, however, gives a significantly lowered yield of triterpenoids and suggests that components can be chemically incorporated into the DBC by this process, once again implicating oxygenated functional groups in densification.

Acknowledgement.

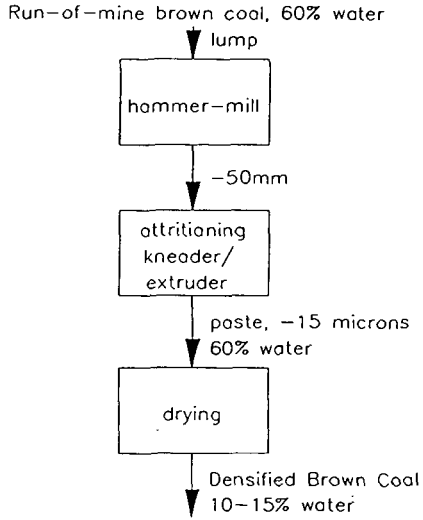
The authors thank CRA - Advanced Mineral Chemistry for financial support.

References

1. George, A.M., SEC of Victoria, Petrographic Report No.17, 1975.
2. Perry, G.J. and Allardice, D.J., Coal Res. Conf. N.Z., 1987, Proc.I, Sec.4., Paper R4.1.
3. Johns, R.B., Verheyen, T.V. and Chaffee, A.L., Int. Conf. Coal Sci. Dusseldorf 1981, 863-868.
4. Johns, R.B., Chaffee, A.L., Harvey, K.F., Buchanan, A.S. and Thiele, G.A., Fuel Proc. Techn. 1989. In the press.
5. For example, U.S. Patents 4,627,575 and 4,701,184.
6. Verheyen, T.V. and Johns, R.B., Geochim. Cosmochim. Acta, 1981, **45**, 1899-1908.
7. Verheyen, T.V., Johns, R.B. and Espitalie, J., Geochim. Cosmochim. Acta, 1984, **48**, 63-70.
8. Hodges, S., Woskoboenko, F., Stacy, W.O. and Brockway, D.J., Aust. Coal Sci. Proc. 1988, Paper A4:2.1.

FLOW CHART FOR DENSIFICATION

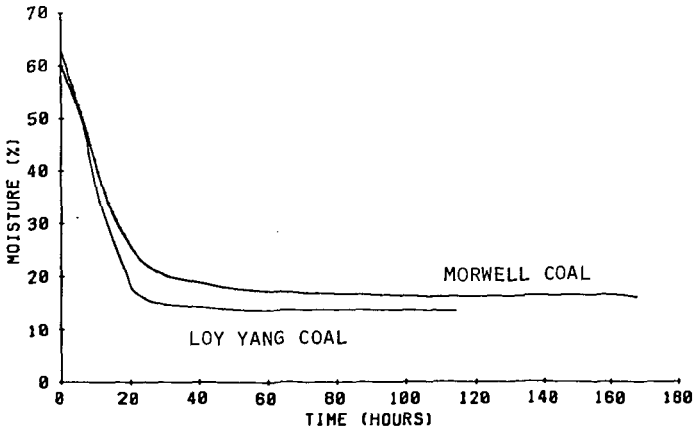
FIGURE 2



MOISTURE LOSS CURVES

FIGURE 3

DRYING AT 20° C AND 50% REL. HUMID.



PELLET DIAMETER vs DRYING AT 20°C AND 50% REL. HUM.

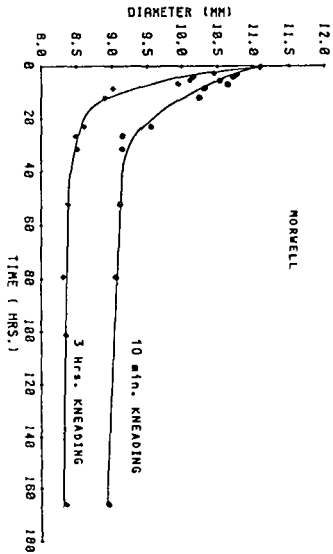
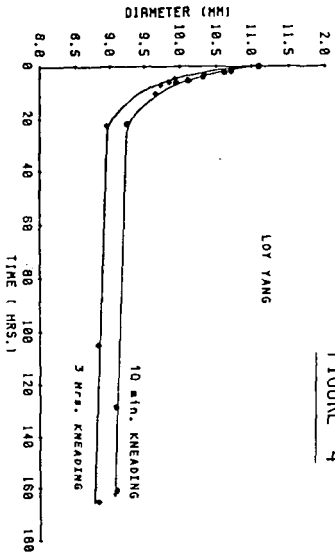


FIGURE 4



CRUSH STRENGTH vs DRYING AT 20°C AND 50% REL. HUMIDITY

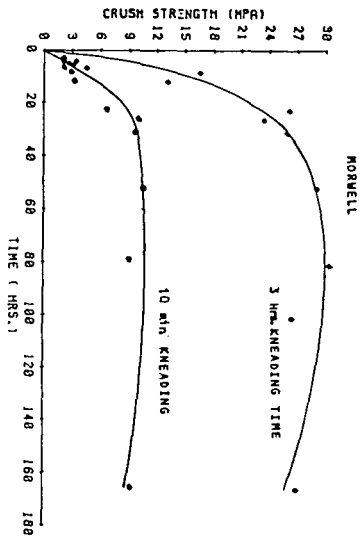
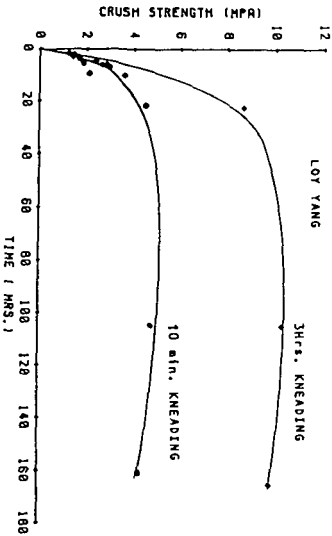
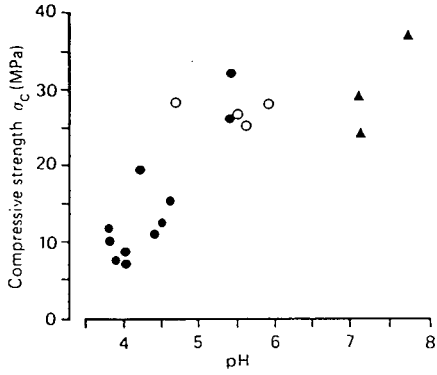


FIGURE 5





● LOY YANG COAL ○ MORWELL COAL
 ▲ MADDINGLEY COAL

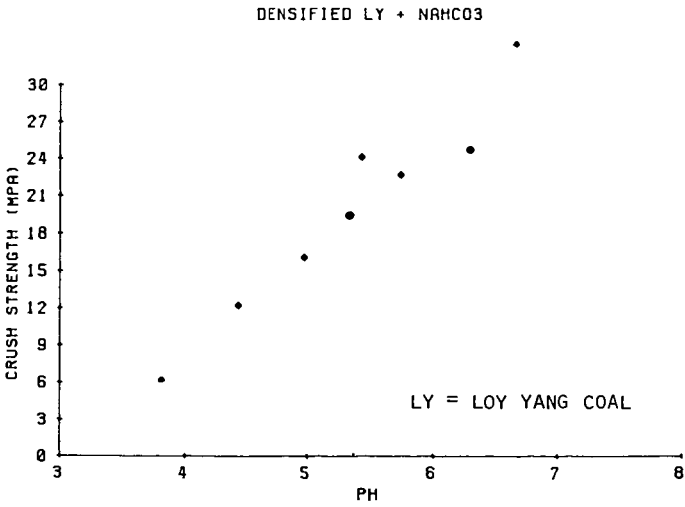


FIGURE 6. TYPICAL PH EFFECTS ON CRUSH STRENGTH

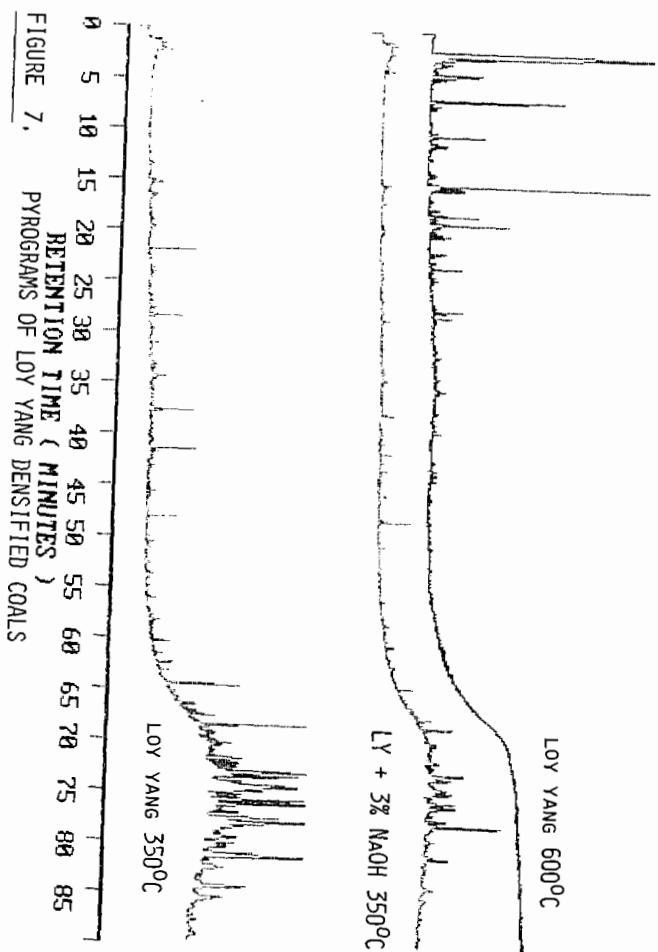


FIGURE 7. PYROGRAMS OF LOY YANG DENSIFIED COALS

ROLE OF PYRITE DURING THE THERMAL DEGRADATION OF KEROGEN
USING IN-SITU HIGH TEMPERATURE ESR TECHNIQUE

By

M. Bakr¹, M. Akiyama², T. Yokono¹ and Y. Sanada¹

Metals Research Institute, Faculty of Engineering¹, and Geology
and Mineralogy Department, Faculty of Science², Hokkaido
University, Sapporo, 060 Japan

INTRODUCTION

Thermal maturation of kerogen in sedimentary rocks has been studied extensively with the intent of better understanding the generation and accumulation of oil and gas (1, 2). The influence of mineral matrices on kerogen during thermal maturation has also been studied. The available in literatures have shown that the role of catalysis in pyrolysis reactions have been directed towards using minerals, such as kaolinite, montmorillonite and calcite (3-7). Analytical techniques applied in these studies did not included in-situ ESR spectroscopy. Moreover, the relationship between pyrite and kerogen has received no attention considering a possible catalytic role of pyrite on the thermal degradation of kerogen. The genetic relationship between pyrite and kerogen, in addition to the evidence that pyrite whether indigenous or added, enhances coal conversion and improves product quality under hydroliquefaction conditions (8-11) makes one wonder whether pyrite also plays a role in kerogen maturation. In this work, in-situ ESR studies between room temperature and 700 °C on the pyrolysis of kerogen in the presence and absence of added pyrite

are reported.

EXPERIMENTAL

Samples studied here include lignin, natural and artificial kerogen. Lignin is a pure reagent supplied from Tokyo Kashei Kogyo. Natural kerogen samples were taken from the MITI-Hamayuchi borehole and Oashizawa outcrops in Japan. Artificial kerogen was prepared from a mixture of glucose and casein (12). Pyrite is a reagent supplied from CERAC, Inc., and was checked with X-ray diffraction and Mossbauer spectroscopy before use. Procedures of Kerogen demineralization and extraction with organic solvents, have been discussed previously (13). The procedure of in-situ high temperature ESR measurements of kerogens has been described elsewhere (14). Since pyrite cannot be fully removed without specific alteration of kerogen structure, no attempts have been made to remove pyrite from the natural kerogen under investigation. Therefore the role of the indigenous pyrite cannot be justified in this study, and discussion will be focused on the added pyrite. To check the catalytic effect of added pyrite on the formation of free radicals, lignin and artificial kerogen as pyrite free materials were tested with and without addition of pyrite.

RESULTS AND DISCUSSION

Fig. 1 shows the temperature dependence of radical concentration for lignin with and without addition of pyrite. There are two significant points that should be mentioned:

(1) the maximum value of spin concentration for pyrite-lignin system is larger than that of the lignin one. (2) pyrite speeds up the process of radical formation, where the maximum value of spin concentration of the lignin-pyrite system is shifted significantly to lower temperature, from 575 °C to 550 °C.

In Fig. 2, the temperature dependence of radical concentration for artificial kerogen alone and the same kerogen with 10% FeS_2 is illustrated. The main effects of pyrite on the thermal decomposition of kerogen are manifested by:

1. A drastic enhancement in radical concentration that starts from 225 °C and proceeds throughout the course of pyrolysis. This enhancement becomes intensive at 450 °C (the temperature of R_3) and drops after that.
2. Speeding up the process of pyrolysis. This causes shift of the ESR maxima (R_1 and R_3) and ESR minimum (R_2) to lower temperatures. Lowering in temperatures was measured as 25 °C for both R_1 and R_2 , and 50 °C for R_3 .

Using the in-situ ESR technique, it has been shown that kerogen maturity and hydrocarbon generation are linked to an extent to that of free radicals therein (15). Fig. 3 demonstrates the temperature dependence of radical concentration for kerogen from Oashizawa outcrops with and without addition of pyrite (10% and 30% FeS_2). In the 10% FeS_2 system, enhancement of radical concentration starts at 275 °C and continues throughout pyrolysis. As for the 30% FeS_2 system, the observed enhancement of the radical concentration starts earlier at 200 °C and becomes more pronounced than that in 10% FeS_2 . Pyrite accelerates the process of radical formation in kerogen. This is manifested by shifting the temperature of the maximum value of radical concentration to lower temperature when pyrite was added. The larger the amount of pyrite is used, the more the shift in the temperature of the ESR maximum can be observed. This shift in temperature follows the sequence kerogen-30% FeS_2 > kerogen-10% FeS_2 > kerogen.

Five kerogen samples from MITI-Hamayuchi borehole were mixed with 10 and 30% FeS_2 and examined by ESR. These samples ranges in

depth from 904 to 4499 meters, and covers the diagenesis and beginning of catagenesis. The temperature dependence of radical concentration for Hamayuchi kerogens in the presence and absence of pyrite as an additive is shown in Figs. 4 and 5 for the shallowest (No. 1) and deepest (No. 5) sample, respectively.

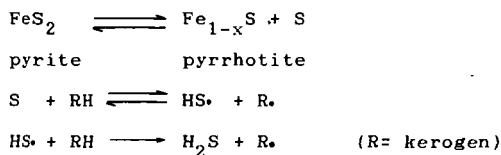
Pyrite in the diagenesis stage. This stage is represented by two samples (Nos. 1 and 2). In sample No. 1 (Fig. 4), the free radical concentration markedly increases in the presence of 10% FeS_2 than in the case when kerogen was pyrolyzed without the additive. When 30% FeS_2 was used, an incremental enhancement in reactivity over the 10% FeS_2 was observed. The overall order of activity in terms of increasing spin concentration is as follows: kerogen-30% FeS_2 system > kerogen-10% FeS_2 system > kerogen alone, clearly indicating the strong effect of FeS_2 during the pyrolysis of kerogen. Also speeding up the process of radical formation can be observed as the temperature at the positions of the maximum values of spin concentration is shifted to lower temperature when pyrite was added. Similar results were obtained for sample No. 2.

Pyrite in the catagenesis stage. The beginning of catagenesis is represented by three samples (Nos. 3, 4 and 5). Fig. 5 shows the results of sample No. 5. There is no noticeable change in spin concentration using 10% FeS_2 , where the spin concentration in kerogen alone fraction and kerogen-10% FeS_2 one is nearly the same. However, slight increase in spin concentration was observed in the presence of 30% FeS_2 as is shown in Fig. 5 for sample No. 5. This results provide evidence that the effect of pyrite in this stage is either small (for 30% FeS_2 system) or negligible (for 10% FeS_2 system) comparing with the diagenesis stage. Similar results were obtained for samples Nos. 3 and 4.

Decomposition of indigenous pyrite in kerogen. Three sets of

heating experiments were carried out on kerogen sample No. 1. at 325, 375 and 450 °C in N₂ atmosphere. X-ray diffraction and Mossbauer showed transformation of indigenous pyrite to pyrrhotite at 450 °C.

Decomposition of reagent pyrite. Five sets of experiments have been conducted in N₂ atmosphere at 250, 375, 425, 475 and 550 °C. The transformation of pyrite to pyrrhotite was commenced at 250°C. This transformation process becomes more significant as the temperature increases to 550 °C. Thus it is evident that the large enhancement in radical concentration observed in the lignin-pyrite system (Fig. 1), artificial kerogen-pyrite system (Fig. 2) and natural kerogen-pyrite systems (Figs. 3 and 4) is consistent with the conversion of pyrite to pyrrhotite. The increase in radical concentration with FeS₂, may be attributed to the nascent sulfur produced during the process of conversion of pyrite to pyrrhotite. The pyritic sulfur is a strong hydrogen acceptor, where it may abstracts hydrogen from kerogen via a free radical process. This process of radical formation may takes place as follows:



The enhancement of free radical formation via hydrogen transfer from kerogen (as a hydrogen donor) to sulfur (as a hydrogen acceptor) is illustrated in Fig. 6. Clearly, S is acting as a catalyst for generation of radicals in kerogen at these conditions. It should be noted that similar enhancement of radical formation by the catalytic effect of pyritic sulfur have been observed for coal (15).

Hydrocarbon generation and the role of pyrite. Hydrogen and carbon atoms crack from kerogen to form petroleum. This cracking process proceeds via free radicals formation. The more hydrogen a kerogen contains, the more hydrocarbon it can yields during cracking, and the more activity of pyrite can be observed. With increasing burial depth in Hamayuchi samples, the aliphatic hydrocarbons decrease. FT-IR data shows that the intensity of the aliphatic portion of kerogen carbon (CH) between 3000-2700 cm^{-1} in sample No.1 is larger than that in sample No. 5. Elemental analysis also shows that sample No. 1 is richer in hydrogen than sample No.5. This may be the reason responsible for the activity of pyrite in sample No. 1.

CONCLUSION

Based on the data presented in this study, pyrite acts indirectly as a catalytic agent via sulfur. Pyritic sulfur enhances the formation of free radicals which may reflect enhancement in the hydrocarbon generation.

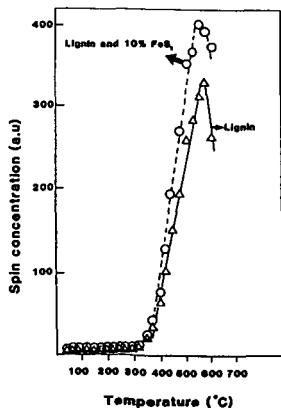


Figure 1. The temperature dependence of radical concentration of lignin in the presence and absence of FeS_2 .

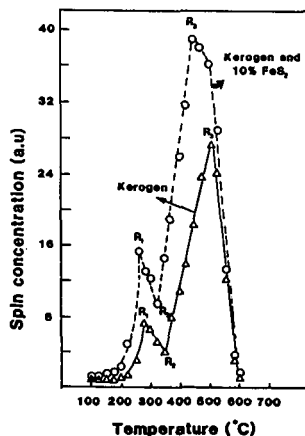


Figure 2. The temperature dependence of radical concentration of artificial kerogen in the presence and absence of FeS_2 .

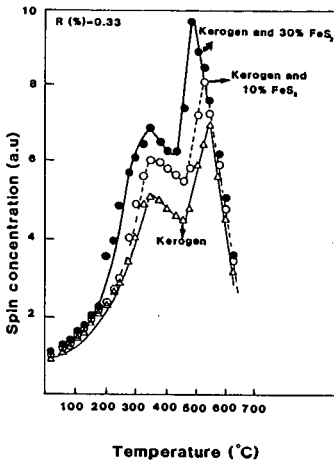


Figure 3. The temperature dependence of radical concentration of Oashizawa kerogen in the presence and absence of FeS_2 .

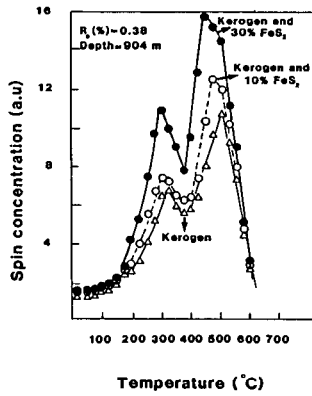


Figure 4. The temperature dependence of radical concentration of Hamayuchi kerogen No. 1 in the presence and absence of FeS_2 .

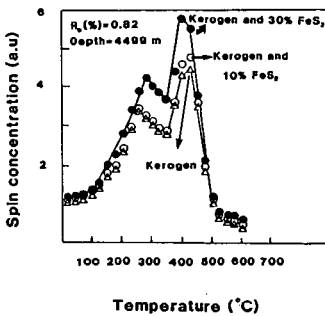


Figure 5. The temperature dependence of radical concentration of Hamayuchi kerogen No. 5 in the presence and absence of FeS_2 .

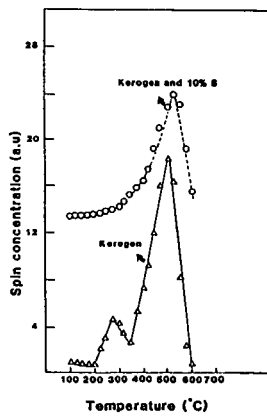


Figure 6. The temperature dependence of radical concentration of artificial kerogen in the presence and absence of sulfur.

LITERATURE CITED

- (1) Tissot, B. P. and Welte, D. H. Petroleum formation and occurrence, Berlin, Springer-Verlag (1984).
- (2) Hunt, J. M. Petroleum geochemistry and geology, San Francisco, Freeman (1979).
- (3) Evans, R. J. and Felbeck JR, G. T. Org. Geochem. 4, 3/4, 145 (1983).
- (4) Espitalie, J., Makadi, K. S. and Trichet, J. Org. Geochem. 6, 365 (1984).
- (5) Tannenbaum, E. and Kaplan, I. R. Geochim. Cosmochim. Acta. 49, 2589 (1985).
- (6) Huizing, B. J., Tannenbaum, E. and Kaplan, I. R. Org. Geochem. 11, 6, 591 (1987).
- (7) Huizing, B. J., Tannenbaum, E. and Kaplan, I. R. Geochim. Cosmochim. Acta. 51, 1083 (1987).
- (8) Baldwin, R. M. and Vinciguerra, S. Fuel, 62, 498 (1983).
- (9) Sondreal, E. A., Willson, W. G. and Stenberg, V. I. Fuel, 61, 925 (1982).
- (10) Stohl, F. V. Fuel, 62, 122 (1983).
- (11) Alexander, B. F. and Anderson, R. P. Am. Chem. Soc. Div. Fuel Chem., Prepr. 27, (2), 18 (1982).
- (12) Yamamoto, S. Ph.D. Thesis, Tokyo Metropolitan University (1983).
- (13) Bakr, M., Akiyama, M., Yokono, T. and Sanada, Y. Org. Geochem. 12, 1, 29 (1988).
- (14) Bakr, M., Akiyama, M. and Sanada, Y. Submitted to Fuel & Energy (1989).
- (15) Bakr, M. Y. Ph.D. Dissertation, Hokkaido University, Sapporo, Japan (1988).

Minerals and Inorganics Associated with South Australian Lignites

Keith B. Quast and David J. Readett

Metallurgy Department, S.A. Institute of Technology,
The Levels, South Australia 5095, Australia

INTRODUCTION

South Australia is endowed with considerable reserves of low rank Permian to Jurassic sub-bituminous coal and Tertiary lignite. A number of these occurrences have been evaluated since the mid 1970's to assess their suitability for power generation. Of the lignites, the Bowmans (1,600 Mt) and Lochiel (580 Mt) deposits from the Northern St. Vincent Basin have been the subject of extensive research. Both these lignites contain in excess of 50% moisture and very high Na, Cl, and S contents, all of which create problems for any subsequent utilization. Combustion trials on both Bowmans and Lochiel lignites have been conducted as well as pilot scale gasification and circulating fluidized bed combustion tests. As a consequence of this work it has been realised that the non-carbonaceous component of the lignite presents major technical and economic problems.

In the light of this, an extensive research program has been conducted at the S.A. Institute of Technology to determine both the minerals and inorganics present and their distribution in South Australian lignites. A major part of this project was the development of techniques to enable the analysis of minerals using Scanning Electron Microscopy (SEM) with Back Scattered Electron (BSE) imaging, Energy Dispersive X-Ray Spectrography (EDS), X-Ray Diffraction (XRD) and mechanical dewatering to extract water for subsequent analysis.

LITERATURE REVIEW

The occurrence of non-carbonaceous material in coals has been the subject of much research, especially in relation to its effect on utilization and ash formation ((1)-(7)). In contrast to high rank coals where the coal mineral matter represents the total non-carbonaceous fraction, the low rank coals have two categories of non-carbonaceous material : minerals (discrete particles e.g. quartz, marcasite, clays, etc) and inorganics (water soluble salts and exchangeable ions e.g. NaCl, Na₂SO₄, Al³⁺, etc.) ((8), (9)).

Much of the literature published on minerals is based on high rank coals, but can be related to low rank coals ((10)). In general, the silicate minerals represent the major component of the minerals contained in coal. The most common analytical methods for mineral characterisation and analysis are listed in Harvey and Ruch (11) and covered in detail in the "Analytical Methods for Coal and Coal Products" series (12).

The majority of the early studies on inorganics was based on the determination of the chloride content, its mode of occurrence, and why it was present (13). It is only in more recent years with the increase in low rank coal utilization where the inorganics have a considerable economic impact that detailed research on inorganics has been undertaken ((9), ((14)-(17))). This work indicates that the inorganics in low rank coals exist in two forms: as free ions present in the water associated with the coal and as cations exchanged on to the surface functional groups of the coal. Analysis of the inorganics is most commonly done using leaching to extract the inorganics, followed by Atomic Absorption techniques for cations and standard chemical analysis for anions.

Samples

Typical analyses of the four South Australian lignites are given in Table 1. They are ranked as Lignite B on the ASTM system.

Table 1 South Australian Lignites*

	Bowmans	Lochiel	Sedan	Kingston
Moisture	56	61	59	53
Higher Heat Value (wet basis)(MJ/kg)	10.6	9.1	9.1	10.6
% Ash (db)	14	16	20	15
% Vol. Matter (db)	46.7	49.9	43.9	46.9
% Sulphur (db)	5.0	2.8	5.5	2.9
% Sodium (db)	1.55	0.95	0.60	0.85
% Chlorine (db)	1.5	0.5	0.25	0.15
<u>Ultimate Analysis</u>				
% C	59.7	57.8	54.7	59.2
% H	3.9	4.7	4.1	4.1
% N	0.4	0.6	0.5	0.6
% O	17.0	18.2	15.0	18.3

* Data from the Electricity Trust of South Australia

TECHNIQUES USED IN THIS STUDY

SEM-BSE /SEM-EDS

A Cambridge Stereoscan 100 Scanning Electron Microscope with a KEVEX Energy Dispersive Spectrography unit was used in all the experimental work. In order to ensure optimum conditions for the analysis, it was necessary for the lignite samples to be in the form of a polished section. Lignite samples were crushed to all passing 2mm and allowed to air equilibrate at 20°C for 2 days. These partially dried samples were then impregnated with epoxy resin. After the resin had set, each sample was polished using diamond paste and kerosene as a lubricant. Prior to viewing under the SEM, each polished section was coated with a fine layer of amorphous carbon using a vacuum arc coater to ensure adequate electrical conductivity to prevent charging.

To enable detection of fine mineral particles, (<20µm) back-scattered electron imaging was used. Once the minerals were detected, the EDS was used for analysis. Selected lignite particles were scanned to determine the distribution of minerals. Mineral types were then differentiated by variation in back scatter intensity and identified using the EDS. The relative proportions (major, minor) and size distributions of the minerals were recorded. The overall surface of the polished section was viewed and "massive" minerals were analyzed and their distribution and size recorded.

Inorganic analysis was conducted in conjunction with the mineral analysis. Particles analyzed previously for mineral content were analyzed for their inorganic content, and an overall analysis conducted. The resultant EDS spectra output was fed into a spreadsheet software package which was adapted by the authors to allow the calculation of a quantitative elemental analysis.

X-Ray Diffraction

Lignite samples were predried at 105°C for 2 hours to remove the water which is a major impurity component, hence its removal in effect concentrates the mineral species. After drying, the samples were crushed using a mortar and pestle until all passing 75µm. The dried lignite powder was then mounted in a standard aluminium mounting plate and placed in a Philips X-ray Diffractometer with a Rigaku power source. A Co X-ray tube was used to suppress fluorescence of any elemental species. The resultant diffraction pattern was resolved using the JCPDS Fink and Hanawalt Indexes.

Leaching

Standard procedures using leaching for determining inorganic species in low rank coals are well established. The procedures adopted for this study are given below. All lignite samples were crushed finer than 1mm and dried at 105°C for 2 hours. Samples weighing 2g were mixed with 100ml of distilled water and agitated for 1 hour. The resultant slurry was filtered and analyzed. The amounts of water soluble inorganics were calculated on a dry coal basis. For the acid extraction, 100ml distilled water and 15ml concentrated A.R. nitric acid were added, and the slurry boiled and simmered for 1 hour on a hot plate. The resultant slurry was filtered and analyzed to allow total inorganics present in the sample to be calculated.

Mechanical Dewatering

The analysis of water soluble inorganics present in the lignites can be calculated from the analysis of water contacted with the lignite as described above. It is uncertain whether water leaching induces any chemical changes (e.g. dissociation of ions from the surfaces of lignite or minerals, etc.). It was therefore considered that a more appropriate means of determining the analysis of water soluble inorganics would be to remove the water from the lignite by mechanical means. Design of equipment capable of mechanically dewatering lignites was obtained from the Grank Forks Energy Technology Centre and CSIRO. Using these designs as a basis, a mechanical press was constructed. The basic criterion for design was that it would dewater a sufficiently large sample of lignite to obtain a suitable volume of water for subsequent analysis.

All the lignite samples were initially crushed to pass 1mm and contact with the atmosphere was kept to a minimum. A lignite sample was placed in the die. The punch (which transfers the pressure from the Avery machine to the lignite) was then placed in the die. The lignite was then pressed against a series of water permeable screens and drainage plates. Under the applied pressure, water was expressed from the lignite sample and exited the dewatering device via the screens and drainage plates, whilst the dewatered lignite was retained on the screens. The expressed water was analyzed by conventional means.

RESULTS

The inorganics content of the lignite samples is given in Table 2 with the minerals and their distribution given in Table 3.

Table 2 Extractable Inorganics

SAMPLE	EXTn	COMPOSITION (%db)								
		Na	Ca	K	Mg	Fe	Al	Cl	S	SiO ₂
Bowmans	Acid	1.86	0.62	0.05	0.83	1.06	0.28	2.23	3.34	0.53
	Water	1.52	0.10	0.02	0.26	-	0.01	1.98	0.73	0.01
	Press	0.93	0.08	0.01	0.26	-	-	1.90	0.40	-
Lochiel 1	Acid	1.52	0.95	0.05	0.80	0.35	0.28	0.16	2.18	0.41
	Water	1.33	0.02	0.02	0.04	-	-	0.92	0.56	0.01
	Press	0.82	0.07	0.01	0.21	-	-	1.15	0.43	-
Sedan	Acid	0.39	1.59	0.05	0.52	2.16	0.42	0.01	4.32	0.68
	Water	0.39	1.30	1.12	1.19	0.02	0.17	0.12	3.87	0.04
	Press	0.23	0.05	-	0.55	0.08	0.15	0.11	1.38	0.03
Kingston 1	Acid	1.11	1.30	0.12	1.19	0.02	0.27	0.01	1.23	0.42
	Water	0.28	-	0.01	-	-	-	0.24	0.07	0.01

Acid - acid extractable inorganics

Water - water extractable inorganics

Press - inorganics removed by mechanical dewatering.

Table 3 Minerals and Distribution in Lignite Samples

SAMPLE	DISTn	DENSITY	DISTn	MINERAL SPECIES			
				Major	Size Range (µm)	Minor	Size Range (µm)
BOWMANS	-2+0.21mm	medium	even	Si	-500	CaS	-200
				Al, Si	-500	Fe, S	-200
-0.21mm	medium	uneven	Al, Si	-150	CaS	-100	
			Si	-150	NaCl	- 5	
			FeS	-150			
LOCHIEL 1	-2+0.21mm	low	uneven	Si	-500	Fe, S	-200
						Ca, S	-200
-0.21mm	low	uneven	Si	-200	Fe, S	-100	
			Al, Si	-200			
LOCHIEL 2	-2+0.21mm	medium	even	Al, Si	-200	Fe, S	-200
				Si	-500	Ca, S	- 5
KINGSTON 1	-2+0.21mm	medium	even	Si (acic)	- 20	Ca, S	- 20
				Al, Si	-200	Na, Al, Si	-150
-0.21mm	low	uneven	Si (acic)	- 20	Al, Si	- 20	
					Na, Al, Si	- 50	

KINGSTON 2			Si (acic)	- 20	Na,Al,Si	-200
-2+0.21mm	medium	uneven	Al,Si	-500	Fe, S	-200
					Ca, S	- 20
SEDAN			Si	-500	Fe, S	-500
-2+0.21mm	low	even	Ca, S	-500		
			Al, Si	- 50		
-0.21mm	medium	uneven	Ca, S	-200	Fe, S	-200
					Si	-150
					Al, Si	-150

Key to Table 3

Elements detected	Species	Elemental Analysis
Si	quartz	SiO ₂ *
Si(acic)	acicular quartz	SiO ₂
Fe, S	marcasite	FeS ₂ *
Ca, S	gypsum	CaSO ₄ .2H ₂ O*
NaCl	halite	NaCl
Al, Si	kaolinite	Al ₂ O ₃ .2SiO ₂ .2H ₂ O*
Na, Al, Si	plagioclase	Na ₂ O.Al ₂ O ₃ .6SiO ₂

* elements detected using XRD

DISCUSSION

Analytical Techniques

The procedures developed for the analysis of the minerals and inorganics were the result of an extensive series of scouting tests to determine the optimum conditions for these specific sample types. This was then combined with general procedures for the analytical equipment (i.e. SEM-EDS and XRD units).

SEM-EDS

The equipment and procedure used had several inherent problems including:

1. Poor sensitivity of the EDS for elements of low atomic number (especially Na and Mg) and an inability to detect elements with atomic numbers less than 10. The software can derive quantitative analysis from a spectrum taking into account the inherent insensitivity of the EDS to those elements whose atomic numbers approach the detection limit.
2. The detection difficulties were then accentuated by the characteristic background x-ray spectrum which was superimposed on the x-ray spectrum of interest. This was overcome by the modelling and subtraction of the background from the acquired x-ray spectrum.
3. Preliminary tests indicated that the distribution of inorganics within a particle could be a function of the rate at which the lignite sample was dried. Rapid drying rates resulted in a concentration of inorganics in the central zone of a particle, whereas slow drying rates resulted in a concentration at the outer perimeter of the particle.
4. To enable quantitative analysis of the inorganics it is necessary to have a known standard. Chemical analysis of the sample to determine the concentration of one species i.e. Cl or S etc. will give a suitable standard.

5. The analysis does not distinguish between minerals and inorganics in the lignite. Despite these drawbacks, it was possible to detect trends occurring in the inorganics associated with the lignite

The technique of BSE images on the SEM screen was ideal for the detection of minerals in low rank coals. The difference in atomic number between the major components of the coal matrix (i.e. C, H, N and O) and the elements present in the mineral species (i.e. Si, Al, Fe, Ca) means that the minerals fluoresce against the dark coal background. Variations in the BSE intensity between minerals was such that the different minerals present were also detectable. Using this technique, however, does in some cases make it difficult to differentiate between quartz and clay (kaolinite) just from a BSE image.

This problem can be overcome to an extent by differentiating between the actual crystal structure which is apparent between quartz, clay and other minerals.

A secondary problem occurs as the low density of the coal matrix allows for a beam penetration to a depth of approximately 10µm. This means that the BSE image represents a surface volume rather than just a plane. Minerals which are subsurface are therefore visible, however their intensity is diminished (e.g. subsurface marcasite can have a similar BSE intensity to clay on the surface).

Analysis of the minerals detected using SEM-EDS was effective with simple minerals, however, determination of clay types was difficult and it was not possible to determine whether a mineral species was anhydrous or hydrated.

XRD

The limitation of an SEM-EDS analysis of minerals is that it cannot characterise the crystal structure of the minerals present. As a result it is difficult to determine some mineral types i.e.

1. differentiating clay types
2. whether the presence of Fe and S is indicative of pyrite, marcasite or FeSO₄.
3. minerals which have anhydrous and hydrated forms.

XRD allows the determination of the actual mineral species present. The bulk coal samples resulted in an x-ray pattern with a high background due to the coal matrix. The major mineral species were easily determined however, the minor species could not be detected. As with the SEM-BSE analysis, interpretation of results in a quantitative manner (in relation to the coal) is difficult. The major mineral species detected were quartz, kaolinite, gypsum (CaSO₄.2H₂O) and marcasite (FeS₂).

Minor mineral species were not detected as their concentration in the samples was below the detection limits for XRD.

Leaching

The limitation of water leaching is that some species which are not soluble within the coal sample may dissociate on leaching. For the acid leaching, a major problem arises from the dissolution of mineral species. This means that both cations exchanged onto the surface are removed as well as ions from the minerals and it is not possible to determine the amount of ions related to the two different environments.

Mechanical Dewatering

The design of the mechanical dewatering press is such that there is a limit to the pressure under which the lignite is subjected. The dewatering pressure is one of the major factors determining the extraction of water, and a suitable sample of mechanically removed water

could not be obtained from the Kingston sample. Overall the technique was successful and several good water samples were obtained from the Bowmans, Lochiel and Sedan samples.

Data Obtained on South Australian Lignites

Inorganics

The inorganics analysis given in Table 2 show that all of the South Australian lignites have high Na, Cl and S contents. The Bowmans lignite has the highest Na and Cl levels of 1.86% and 1.98% respectively.

In general the water soluble inorganics consist of predominantly Na, Cl and S (as SO_4^{2-}) with lesser amounts of Ca and Mg. The Bowmans and Lochiel lignites, both from the St. Vincents Basin, have very high Na, Cl and S as a consequence of the saline environment in this region. The Sedan lignite in contrast has very high Ca and Mg concentrations (1.3 and 1.19% respectively). The Kingston lignite exhibits a relatively low concentration of water soluble inorganics.

Acid leaching results give an indication of the total inorganics present in the coals, including:

- water soluble ions;
- cations exchanged onto the surface functional groups associated with the coal;
- cations exchanged onto the clay minerals
- ions emanating from the dissolution of hydrolysis of minerals.

The water soluble component is easily differentiated, however the other three are not. For the Bowmans, Lochiel and Sedan lignites the acid soluble components (i.e. total inorganics - water soluble inorganics) are predominantly cations (Na, Mg, Ca, Al and Fe) which are exchanged onto the lignite surface. In contrast, for Kingston lignite which has the highest acid soluble component, inorganics are (compared with the water soluble component) associated with ions associated with or exchanged in the clay minerals.

Analysis of the mechanically removed water showed some significant variations especially with respect to Na. It can be seen that for Bowmans, Lochiel and Sedan lignites, the Na content detected by mechanical removal of water is noticeably less than that for the water soluble Na. This aspect of the occurrence and distribution of Na (and Cl) within these samples was discussed in detail in a paper presented by the authors recently (17). The distribution of Na was found to be a function of the high negative surface charge of the coal surface resulting in adsorption of Na at this surface.

Minerals

All of the samples analysed showed, as expected, that the major mineral species were quartz and kaolinite (syngenetic), marcasite and gypsum (epigenetic). In general the quartz was present in two distinct size ranges: 500 μm and 50 μm .

One major variation was noted in the two Kingston samples where the majority of the quartz was acicular in form and -20 μm in size. The size distribution of the kaolinite was quite variable and again the Kingston sample differed in that most of the kaolinite had Na associated with it. Marcasite was commonly present as an intimately associated impurity within the coal and in many cases it had replaced the original coal structure (pseudomorphing). The gypsum was present mainly in the -20 μm size range. Overall the mineral matter content of the lignites was in the order of 5-10% (i.e. a medium distribution density).

SUMMARY AND CONCLUSIONS

Minerals and inorganics from the South Australian lignite deposits have been determined using both standard and specifically developed analytical techniques. Techniques used include SEM-BSE/SEM-EDS, XRD, leaching and mechanical dewatering. The inorganics within the lignite samples showed variations between deposits and within the same deposit. Quartz and kaolinite were the predominant mineral species and these also exhibited major variations within and between deposits.

ACKNOWLEDGEMENT

This research was financed by the South Australian State Energy Research Advisory Committee (SENAC).

REFERENCES

- 1) O'Gorman, J.V. and Walker, P.L., Jr. (1972). "Mineral Matter and Trace Elements in U.S. Coals", Coal Research Section, College of Earth and Mineral Sciences, Pennsylvania State University.
- 2) Ward, C.R. (1978). Proc.Australas. Inst. Min. Metall. No. 267, 7-25.
- 3) Miller, R.N., Yarzab, R.F. and Given, P.H. (1979), Fuel, 58, 4-10.
- 4) Berkowitz, N. (1979). "An Introduction to Coal Technology", Academic Press, New York.
- 5) Rigby, G.R. et. al. (1982). NERDDP End of Grant Report, No.144.
- 6) Meyers, R.A. (ed.), (1982). "Coal Structure", Academic Press, New York.
- 7) Raask, E. (1985), "Mineral Impurities in Coal Combustion", Hemisphere Publishing Corp., New York.
- 8) Kiss, L.T. and King, T.N. (1977), Fuel, 56, 340-341.
- 9) Perry, G.J., Allardice, D.J. and Kiss, L.T. (1984). ACS Symposium Series 264, "The Chemistry of Low-Rank Coals", ed. H.H. Schobert, American Chemical Society, 3-14.
- 10) Huffman, G.P. and Huggins, F.E. *ibid*, p.159-174.
- 11) Harvey, R.D. and Ruch, R.R. (1986), ACS Symposium Series 301, "Mineral Matter and Ash in Coal" ed. K.S. Vorres, American Chemical Society, 10-40.
- 12) "Analytical Methods for Coal and Coal Products", ed K.C. Carr (Academic Press), Vol. I (1978), Vol. II (1980) and Vol. III (1981).
- 13) Kear, R.W. and Menzies, H.M. (1965), BCURA, 20, No. 2., p.53-65.
- 14) Kube, W.R., Schobert, H.H., Benson, S.A. and Karner, F.R. (1984), Ref. 9, p.39-51.
- 15) Benson, S.A. and Holm, P.L. (1985), Ind. Eng. Chem. Prod. Res. Dev. 24, 145-149.
- 16) Miller, R.N. and Given, P.H. (1986), Geochim et Cosmochim. Acta, 50, 2033-2043.
- 17) Readett, D.J. and Quast, K.B. (1988), Proceedings, AIE Coal Science Conference 3, Adelaide, Paper A2.3.

ASSOCIATION OF MINERAL MATTER WITH THE ORGANIC COAL MATRIX

Warren E. Straszheim and Richard Markuszewski

Fossil Energy Program, Ames Laboratory,
Iowa State University, Ames, IA 50011.

ABSTRACT

Advances in the quantitative assessment of the association of mineral particles with the organic coal matrix have been made recently at the Ames Laboratory. In addition to routine analysis of mineral matter for particle size and mineral phase, coal particles are classified according to the mass fraction of the various minerals found in cross sections of the particles. Particles are also classified according to the relative amount of mineral matter and coal present on their surface. Examples are given of the resulting distributions for individual minerals showing their liberation, and results are related to coal recovery and ash reduction of the sample during cleaning.

INTRODUCTION

Variations in the characteristics of mineral matter in coal have a significant bearing on the effectiveness of removal of mineral matter during cleaning. The size distributions of the mineral particles play a significant role in determining cleanability since it is generally easier to remove the larger mineral particles. However, it is the association of mineral particles with the organic coal matrix that ultimately determines the cleaning potential. On occasion, certain minerals can be preferentially liberated and then physically removed while others remain associated with the coal matrix.

In practice, coal is not ground to a size at which all mineral matter is liberated from coal; it would not be economically feasible. Rather, coal is processed only to the extent that is necessary to comply with applicable environmental regulations. In this context, it is more important to know to what extent the coal and minerals are still associated.

In the last few years, image analysis techniques have been adapted to the in-situ characterization of the association of individual minerals with coal. Scanning electron microscopy (SEM) is used to observe coal and mineral particles in cross section, energy-dispersive x-ray analysis (EDX) is used to determine the elemental composition of the mineral particles, and automated image analysis (AIA) is employed to characterize a sufficient number of particles for reproducibility. Such techniques have been in use in the mineral industry for many years (1,2). However, the application of these techniques to coal has lagged, partly due to the inability to resolve coal particles from the mounting media. Conventional epoxy resins do not exhibit contrast with coal particles. Therefore, the use of carnauba wax was developed as an alternative and effective medium (3).

METHODOLOGY

Two sets of coal samples were chosen to illustrate applications of AIA to coal processing. The first coal was a 200-mesh sample of Williams Fork Q bed coal from Moffat County, Colorado. The coal is ranked as sub-

bituminous A, with 15.3% moisture, 4.18% ash, and 0.45% total sulfur. The coal was subjected to bench-scale float-sink cleaning at 1.6 sp.gr. in a centrifuge. Samples of the raw coal and the float and sink fractions were then collected for analysis. The full procedure has been described extensively elsewhere (4). The second sample was a 325-mesh sample of Upper Freeport coal with 1.3% moisture, 9.88% ash, and 1.56% total sulfur. The coal was cleaned in two separate tests by float-sink and by froth flotation, as described elsewhere (5). Only samples of the raw coal were available for AIA.

Coal samples with their included mineral matter were prepared for image analysis by mixing samples of the dry coal with polyethylene powder (as a diluent) and molten carnauba wax. Because SEM-AIA is often used to explain behavior under a specific set of processing conditions, samples are typically prepared in the same size in which they are received. Pellets were then cut to expose a vertical cross section and polished using standard petrographic procedures. They were then coated with 150 Å of carbon to provide a conductive surface.

Samples were examined with an electron beam of 15 keV and 0.7 nA at magnifications of 200-500 using the backscattered electron (BSE) signal. Use of the BSE signal permits relatively easy differentiation of minerals and coal from each other and from the carnauba wax using simple brightness thresholds. Coal and mineral particles were characterized for area and perimeter, and information on the relationship of adjoining particles with each other was preserved in the stored data. The amount of surface for each particle in contact with coal, mineral matter, and/or mounting media was recorded. X-ray spectra were then collected for 4 seconds for each of the mineral particles. The integrated intensities for 20 elements were compared with a previously prepared table listing ranges of elemental intensities characteristic of minerals found in coal in order to identify the particles (6,7). Handbook values of mineral densities were then used to convert the results from area fractions to weight fractions, which are of more direct interest in coal preparation.

Results involve very detailed information for the composite coal/mineral particles and their component parts (i.e., size, identification, and surface associations). The analyst can then prepare tables showing the distributions of the sample mass as a function of the appropriate characteristic. These distributions can then be related to processing behavior. Examples of such distributions are given below.

RESULTS AND DISCUSSION

A typical distribution of mineral matter according to particle size and mineral phase is given in Figure 1 for the major phases in the raw sample of Williams Fork coal. Such particle size distributions relative to the size of the coal particles can be used to predict the ash reduction potential, since larger mineral particles are generally more easily removed, while small mineral particles are likely to be associated with the organic matrix and to appear with the clean coal product. As seen in Figure 1, most of the mineral matter in this coal is quite fine and is thus expected to be rather difficult to remove. However, it is not unusual to find minerals, such as those that occur as cleat fillings, that are readily liberated and then removed by cleaning. Such is also the case with the pyrite in this coal. Pyrite particles show a bimodal size distribution in Figure 1. The larger particles are likely candidates for

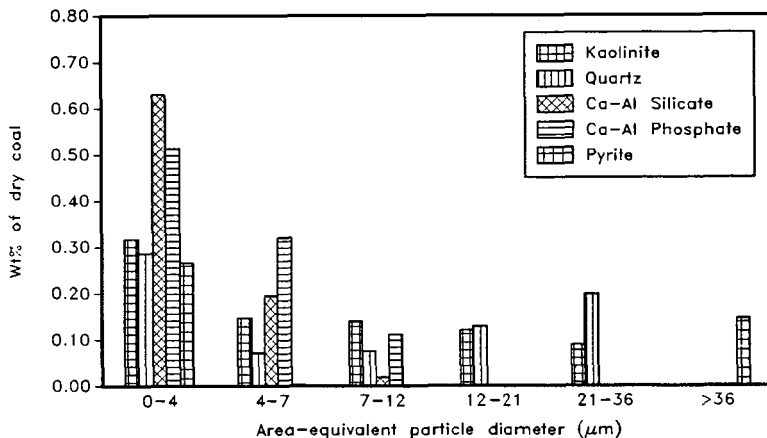


Figure 1. Distribution of selected minerals in raw Williams Fork coal as a function of area-equivalent particle diameter (μm).

removal; however, analysis of the 1.6 sp.gr. float fraction of the coal shows that even small grains of pyrite were removed, implying that they were very well liberated. Such cases point out the need to perform some form of association analysis in order to better characterize the coal.

As one alternative, we have chosen to express the coal-mineral association results in terms of the weight fraction of mineral matter in the particle, as determined from the cross section. This corresponds with the so-called grade distributions used in the mineral industry (1,2). Such a distribution for the same sample of Williams Fork coal is shown in Table 1. The results can also be plotted as done in Figure 2 to show the amount of sample of the indicated grade. Samples with good liberation of minerals from coal show a wide separation between coal-rich material on the left and mineral-rich material on the right side of the figure. In this sample there is much mineral matter found across the entire range of grades, indicating that liberation of mineral matter is not complete at this particle size, and that physical cleaning would therefore be difficult.

The cumulative amount of coal and associated mineral matter, observed in Figure 2, can be used to estimate coal recovery and its anticipated ash content during a density-based separation. However, such a correlation is complicated since the AIA-observed mineral content does not directly reflect particle density. Still, such distributions often show dramatic differences between various coal samples. Similar figures for float or sink fractions can reveal the misplacement of coal- or mineral-rich particles to the wrong fraction so that improvements can be made in the process.

Table 1. Distribution of coal and mineral phases in raw Williams Fork coal as a function of particle mineral matter content.

Coal %	0-9	10-19	20-29	30-39	40-49	50-59	60-69	70-79	80-89	90-99	100	Total
Coal	0.11	0.10	0.19	0.28	0.38	0.54	0.84	2.26	5.36	28.61	54.36	93.03
Pyrite	0.39	0.02	0.00	0.00	0.00	0.00	0.00	0.00	0.00	0.00	0.00	0.41
Kaol.	0.07	0.09	0.11	0.13	0.06	0.10	0.05	0.08	0.06	0.06	0.00	0.81
Quartz	0.23	0.06	0.20	0.03	0.08	0.02	0.03	0.03	0.04	0.04	0.00	0.76
Mont.	0.40	0.01	0.04	0.02	0.01	0.03	0.02	0.02	0.02	0.03	0.00	0.61
Other	1.77	0.39	0.16	0.32	0.28	0.21	0.23	0.32	0.37	0.34	0.00	4.38
Total	2.97	0.67	0.70	0.78	0.81	0.90	1.17	2.71	5.85	29.08	54.36	100.00

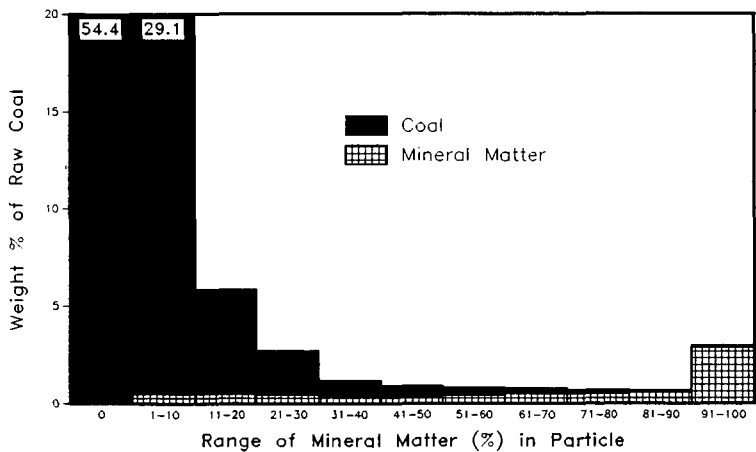


Figure 2. Distribution of coal and mineral matter in raw Williams Fork coal as a function of the particle mineral matter content.

The data of Table 1 can also be plotted for the individual minerals to show variations in the modes of their association, as shown in Figure 3. This figure dramatically shows the difference between pyrite and the other minerals in their association with coal. Pyrite is found exclusively in particles containing more than 80% mineral matter, while the other minerals are associated with particles containing a wide range of mineral matter. From this figure, it appears that pyrite should be easily removed during float-sink separation, which proved to be the case in actual separations, both on a laboratory scale (5) and in practice. Representatives from the mine which produces this coal confirmed that the pyrite occurs as cleat fillings and is rather easily removed (8). Similar

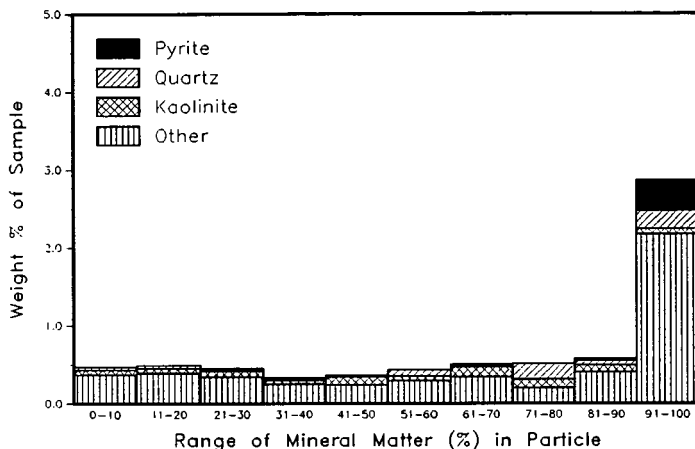


Figure 3. Distribution of minerals in raw Williams Fork coal as a function of particle mineral matter content.

conclusions might be reached by routine manual observation of the polished sections or from operating experience; however, these AIA-SEM techniques permit the measurements to be quantified for comparisons among coals.

In addition to expressing coal-mineral association as a function of particle mineral matter content, as described above using the Williams Fork coal as an example, our recent efforts have emphasized determining association based on particle surfaces. While the previous distributions provide an indication of the probable cleaning behavior of a coal in a density-based process, they do not lend much insight into cleaning behavior during surface-based processes such as froth flotation or oil agglomeration. For such processes it would be better to have results expressed in terms of the proportion of coal (or minerals) present on the surface of the particles. If it were possible to relate floatability to the amount of coal on the surface, then it may be possible to relate cleanability to the AIA-SEM results.

Figures 4 and 5 show the coal-mineral association for Upper Freeport coal based on the mineral weight fraction and the mineral surface fraction of the particles. There is considerable difference between the two figures. While Figure 4 shows that about 74% of the mineral matter is present in particles containing more than 50% mineral matter (i.e., less than 50% coal), Figure 5 indicates that only 10% of the mineral matter is found in particles with less than 50% of the surface covered by coal. Indeed, about 75% of the mineral matter is found in particles with more than 80% coal on the surface. These results indicate that density-based processes (e.g., float-sink) should be able to remove significant amounts of mineral matter, while surface-based processes will likely be unable to

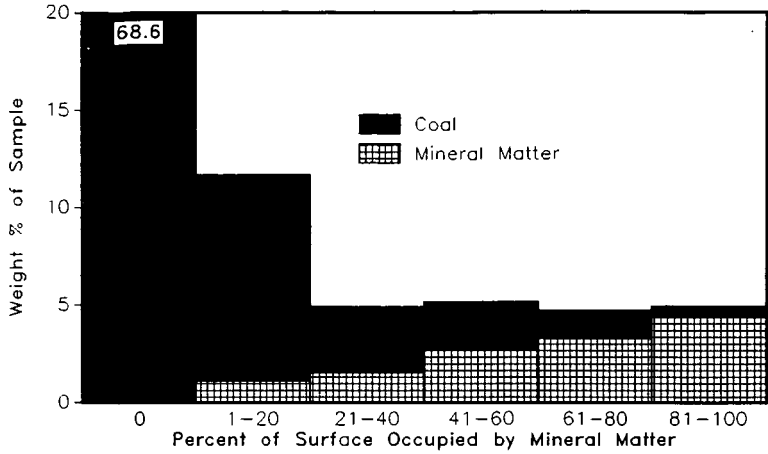


Figure 4. Distribution of coal and mineral matter in raw Upper Freeport coal as a function of particle mineral matter content.

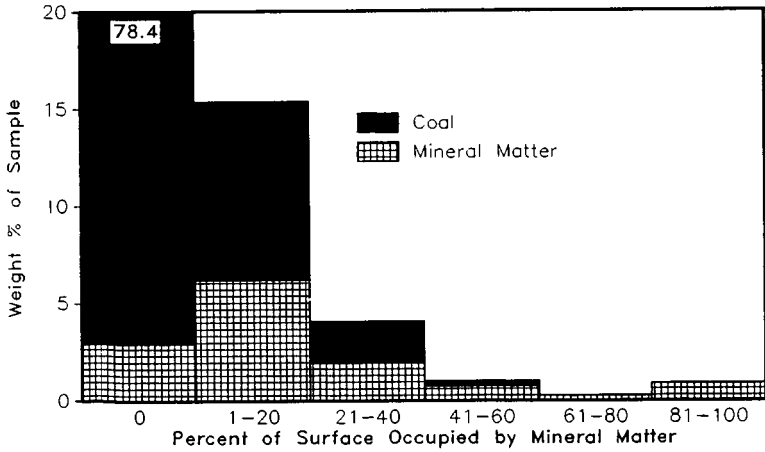


Figure 5. Distribution of coal and mineral matter in raw Upper Freeport coal as a function of particle surface occupied by minerals.

significantly reduce mineral content. Results of cleaning tests reported elsewhere (5) verified these predictions. Float-sink separations at 1.6 sp.gr. reduced the ash content by 57% with a 90% recovery, while froth flotation for 3 minutes resulted in only a 16% reduction in ash content with about the same recovery. Although these AIA results are quite preliminary, they show a strong general correlation with actual cleaning behavior.

SUMMARY AND CONCLUSIONS

AIA-SEM provides insights into coal character and processing potential that are unavailable by other means. Many of the advantages of the technique stem from its ability to characterize coal and mineral particles, in-situ, on a microscopic level. Distributions of mineral matter as a function of particle size and mineral type are readily available and provide some indication of coal cleanability. Results are also now available showing the distribution of phases based on the weight fraction of mineral matter in the particle or based on the relative amount of surface of the particle occupied by mineral matter. These distributions can be related to processing behavior and can be used to explain, and possibly even predict, the recovery and quality of product under various cleaning conditions. The results are especially useful for detecting differences between various coals and for finding the reasons for unusual processing behaviors.

ACKNOWLEDGEMENT

Ames Laboratory is operated for the U. S. Department of Energy by Iowa State University under Contract No. W-7405-Eng-82. This work was supported by the Assistant Secretary for Fossil Energy through the Pittsburgh Energy Technology Center (PETC).

LITERATURE CITED

1. W. Petruk, "Applied Mineralogy in Ore Dressing", in Mineral Processing Design, B Yarar and Z.M. Dogan, eds., Martinus Nijhoff, Boston, 1987, pp. 2-36.
2. A.F. Reid, P. Gottlieb, K.J. MacDonald, and P.R. Miller, "QEM*SEM Image Analysis of Ore Minerals: Volume Fraction, Liberation and Observational Variances", Applied Mineralogy, W.C. Park, D.H. Hausen and R.D. Hagni, eds., The Metallurgical Society of AIME, 1985.
3. W.E. Straszheim, K.A. Younkin, R.T. Greer, and R. Markuszewski, "Mounting Materials for SEM-based Automated Image Analysis of Coals". Scanning Microscopy, 2(3), 1257-1264, (1988).
4. W.E. Straszheim and R. Markuszewski, "Evaluation of Physical Coal Beneficiation Using Computerized Microscopy", Applied Mineralogy, W. Petruk, ed., The Metallurgical Society of AIME, (in press).
5. W.E. Straszheim, K.A. Younkin, R. Markuszewski and F.J. Smit, "Evaluation of Coal-Mineral Association and Coal Cleanability by Using

SEM-based Automated Image Analysis", Am. Chem. Soc. Div. Fuel Chem. Preprints 33(2), pp. 64-72 (1988).

6. W. E. Straszheim, J. G. Yousling, and R. Markuszewski, "Analysis of Ash-Forming Mineral Matter in Raw and Supercleaned Coals by Automated Image Analysis-Scanning Electron Microscopy", in Mineral Matter and Ash in Coal (ACS Symp. Series No. 301), K. S. Vorres, ed., Am. Chem. Soc., Washington, D. C., 1986, pp. 449-461.
7. W. E. Straszheim, "Application of automated image analysis to the study of mineral matter in raw and processed coals", PhD. dissertation, Department of Engineering Science and Mechanics, Iowa State University, Ames, Iowa, 1986.
8. Trapper Mining Company, Colorado, personal communication, March, 1989.

COAL STRUCTURE: THE PROBLEM WITH MINERALS

G. A. Robbins

CONSOLIDATION COAL COMPANY
Research & Development
4000 Brownsville Road
Library, PA 15129

INTRODUCTION

Despite considerable effort to understand the chemical nature of the organic and inorganic portions of coal, and substantial advances in instrumentation and methodologies, much of coal's chemical nature remains intractable. This paper reviews methods and their limitations for the determination of specific minerals in coal, and presents results of efforts at Consolidation Coal Company to develop FTIR methods for routine coal mineralogy.

Mineral matter characterization has received considerable attention. Given and Yarzab (1) discussed the problems posed by mineral matter in various coal analyses. Furthermore, mineral matter complicates the chemical treatment of coal. It also has many adverse effects on commercial coal utilization. Coal consumers pay to ship mineral matter, to accommodate its impact on capital equipment and operations, and to dispose of the resultant ash. The impact of coal minerals on utilization motivated Consol's initial interest in mineralogy (2). The results reported here are from a second phase of the FTIR method development, in which extensive improvements were made to the methods.

EXPERIMENTAL

DESCRIPTION OF SAMPLES

Small Data Set. Low-temperature (plasma) ashes (LTAs) were obtained from ten diverse coal samples (Table 1), ranging in rank from lignite to lvb. Infrared spectra were obtained of duplicate samples of each coal. A separate set of duplicates was generated for four of the coals.

Large Data Set. LTAs were analyzed by FTIR for 50 coals, ranging in rank from lignite to lvb. These were a representative subset of duplicates of 95 unwashed and clean commercial coals from the eastern, midwestern and western U.S. and Alberta, Canada. The 50-coal set contained no duplicates, but different coal samples from the same mine were included.

Reference Minerals. The 42 reference minerals and the mineral classes used are listed in Table 2. Most of the minerals were obtained from Ward's Natural Science Establishment, Inc., Rochester, New York. Many of the silicate minerals were American Petroleum Institute (API) standard samples or their equivalents. Numbers given in the table (e.g., kaolinite 4) refer to the API standard designation.

METHODS

Coals ground to -60 mesh were low temperature (O₂ plasma) ashed for about 100-125 hours for bituminous coals and 200 hours for lower rank coals. Ashing containers were made of Pyrex or ceramic.

Mineral standards were hand crushed to $\sim 1/4$ inch, then ground to a fine powder in a ball or Bleuler mill. The powder was aerodynamically classified, and the finest fraction was collected. This was accepted as a mineral standard if 90% or more by weight was 5 μm and smaller particles. Duplicate 13 mm KBr pellets were prepared and the spectra were weight-scaled by reported techniques (3,4). With one exception, all the mineral standard spectra were averages of spectra from duplicate pellets.

LTA samples were ground for 30 minutes in a Wig-L-Bug (15 mg LTA, 50 mg KBr and 500 mg acetone in an agate vial), dried and stored in a dessicator. 13 mm KBr pellets were made and resulting spectra were weight-scaled (3,4).

All spectra were run on a Nicolet 7199 FTIR spectrometer equipped with a wide-band MCT detector. A Nicolet least-squares analysis program (MCOMP) was modified extensively for efficient use with a large number of reference minerals. The reference mineral with the lowest negative concentration was omitted upon each iteration, until only non-negative results were obtained. Generally 12 to 18 minerals remained in the final calculation.

For PLS or PCR calculations, the spectra were transferred to a DEC VAX 11/750 computer. The PLS and PCR program with cross-validation was provided by David Haaland of Sandia National Laboratory (5).

RESULTS AND DISCUSSION

A CRITIQUE OF METHODS FOR COAL MINERALOGY

This survey of five major methods for coal mineralogy and their limitations includes only methods which can provide a "complete" mineral analysis. Methods of limited applicability, such as Mossbauer, are omitted.

X-ray Diffraction. XRD is the most common method used for coal mineralogy (6,7,8). Its major advantage is the ability to unequivocally identify many minerals. The main disadvantages are: 1) reliance on reference minerals, 2) requires careful attention to sample preparation, and 3) low sensitivity to certain minerals (especially many clays) due to poor crystallinity and to particle orientation effects. Many laboratories analyze a separate concentrated clay fraction (less than 2 μm or 5 μm). However, sensitivity is still low and other limitations may arise: 1) the separated clay fraction may not be representative, and 2) the separation procedure can alter the sample. The original coal, instead of the LTA, can be analyzed by XRD. However, this is not satisfactory, since sensitivity is even lower. An extensive interlaboratory comparison of XRD results with Illinois 6 coal showed highly variable results (7). That study also included results from FTIR, SEM and other methods.

Infrared Spectroscopy. The use of IR (9,10,11,12) and FTIR (3,4) for coal mineralogy has been reported. Painter and coworkers (3) demonstrated that FTIR can provide a virtually complete analysis. Painter, Brown and Elliott (4), and others (9,10,11) discuss sample preparation, reference minerals, and data analysis. The advantages of IR are: 1) high sensitivity to molecular structure, 2) unequivocal identification of a number of minerals, 3) small sample size (a few milligrams), and 4) rapid analysis time (once LTA is available). Disadvantages include: 1) reliance on reference minerals, 2) requires careful attention to sample preparation, and 3) limited selectivity (discrimination among similar minerals).

The problem with limited selectivity includes some of the minerals which are problems for XRD: illite, muscovite, smectites and mixed-layer clays. Poor crystallinity creates problems with both XRD and FTIR. The IR spectrum of an amorphous material lacks sharp distinguishing features but retains spectral intensity in the regions typical of its composition. The X-ray diffraction pattern shows low intensity relative to well-defined crystalline structures. The major problem for IR is selectivity: for XRD it is sensitivity. In an inter-laboratory FTIR comparison (7), two laboratories gave similar results for kaolinite, calcite, and illite, but substantially different results for montmorillonite and quartz.

Electron Beam/X-ray Spectroscopy. Several methods based on point count or automated image analysis (AIA) in scanning electron microscopy-energy dispersive X-ray have been reported (13-18). Point count analysis can determine mineralogy; AIA can also determine the size distribution of the minerals. These methods obtain a point-by-point or particle-by-particle elemental analysis. A mineral distribution and analysis is obtained by classifying each elemental composition into one of the mineral categories. Such methods have several advantages: 1) they can be automated, 2) the composite elemental composition can be checked against that of the bulk sample, 3) it is possible to run coal (not necessary to obtain LTA), and 4) they provide some information on statistical and perhaps spatial, size, or morphological distribution of the minerals. For these reasons, such methods have become more popular in recent years. The major disadvantages are: 1) the chemical information and thus the selectivity is limited, since it uses only elemental composition, 2) it relies on a suitable classification scheme for mineral categories, and 3) data collection can be time-consuming (especially for AIA), requiring many hours per sample.

Optical Microscopy. Optical microscopy is the traditional tool of geologists and petrographers for mineral identification and characterization (19). It has two main advantages: 1) positive identification of minerals can be achieved, and 2) information is obtained on mineral distribution and morphology. However, quantitation is difficult, and the analysis is time-consuming, requires highly trained technicians, and is not amenable to automation. Although in common use in petrographic studies, such methods have been displaced by XRD, IR, and SEM-EDS methods for mineralogical studies.

Thermal Techniques. Thermal techniques, especially differential thermal analysis (DTA) have been used for mineral identification (19) and for coal mineralogy (20). The advantages of thermal techniques are: 1) small sample size, 2) little sample preparation (applicable to whole coals), 3) potentially rapid analysis, and 4) information relevant to combustion behavior may be provided. The disadvantages are: 1) the chemical information is limited, resulting in a lack of selectivity due to overlapping curves for individual minerals, 2) identification/quantification depends on reference minerals (though perhaps less sensitive to such problems than XRD or IR), and 3) it is not developed for quantitative use. Interpretation of thermal data is difficult, but could be improved by appropriate software. Variations, such as using different gases to highlight or suppress features, have been used (20). Detection limits of less than 1 wt % to about 30 wt % were reported for different minerals.

General Comments on Mineralogical Methods. The lack of a measure of quantitative accuracy is a general problem with mineralogy. A major limitation for XRD and IR methods is the use of reference minerals, and the standards used are from geological sources other than the coal analyzed. This limitation

will be avoided by only physical separation of the coal minerals or by data analysis techniques (such as factor analysis) which do not require reference minerals. Many studies have reported successful quantitation of mineral mixtures. This is a necessary, but not sufficient, criterion for a good mineralogical analysis. The differences between mineral mixtures and authentic samples are considerable, and good performance on real samples is not guaranteed. The major limitations of SEM-EDS and related techniques are appropriate classification of the elemental data, and obtaining a statistically sufficient number of data points. For classification of data, factor analysis, cluster analysis, or related multivariate techniques appear to be suitable (21).

The IR methods have progressed from hand-drawn baselines and peak height or area for quantitation, to spectral subtraction, to least-squares methods. Least-squares analysis eliminates the reliance on single peaks for quantitation and the subjectivity of spectral subtraction. However, negative concentration coefficients are a problem with least-squares analysis, since they have no physical meaning. Negative components can be omitted according to some criterion and the least-squares process iterated until only positive concentration coefficients remain. However, this does not ensure that the least-squares solution is a global minimum.

Haaland and coworkers (5) discussed other problems with classical least-squares (CLS) and its performance relative to partial least-squares (PLS) and factor analysis (in the form of principal component regression). One of the disadvantages of CLS is that interferences from overlapping spectra are not handled well, and all the components in a sample must be included for a good analysis. For a material such as coal LTA, this is a significant limitation.

Factor analysis extracts information from the sample data set (e.g., IR spectra) and does not rely on reference minerals. However, because abstract factors have no physical meaning, reference minerals may be needed in target transformations or other procedures to extract mineralogical information. One valuable piece of information obtainable without the use of extraneous data is the number of components required to represent the data within experimental error. Reported applications of factor analysis to mineralogy by FTIR are few (12). However, one commercial laboratory is offering routine FTIR mineral analyses to the petroleum industry, based on related methods (22).

The next section of this paper describes the use of classical least-squares analysis of FTIR data to determine coal mineralogy. This is followed by promising preliminary results obtained using factor analysis techniques.

RESULTS USING CLASSICAL LEAST-SQUARES

Reproducibility. Mineralogical results from the ten-coal set (Table 3) are presented as ranges of values. In most cases, the reproducibility is good. Quartz, for example, shows consistently high reproducibility. However, illite, mixed-layer clays and montmorillonite in the first four coals show high variability. These minerals are similar in composition and spectral features. The variability in the FTIR results for these samples is related to variability in the spectral data. The set of ten duplicate spectra gave a pooled SD of 0.03 abs, while the separate set of four duplicate spectra gave a pooled SD of 0.08 abs. Results from the first four samples in the table included the poorer spectral data, while the results from the last six samples were obtained from the better spectra. The reproducibility for total clay content is good, even when vari-

ability in individual clay concentrations is high. Iron sulfides, oxides and sulfates also show some variability, particularly in the first and fourth samples.

Accuracy. Although there is no way to measure the accuracy of the FTIR mineralogical results, there are three areas in which it can be addressed (2,4). The first method is to compare pyrite results obtained by FTIR with the conventional ASTM determination. The agreement (Figure 1) is quite good over the range of 2.9 to 28.1 wt % pyrite in the LTAs from the ten coals. Similar results were obtained based on the 475-400 cm^{-1} region for a smaller sample set (2). The present results are based on the 1575-400 cm^{-1} range. The good agreement for the present data set is surprising, since the only spectral feature reported for pyrite in the mid-infrared is at ca. 415 cm^{-1} . In these spectra, the noise level is high near 400 cm^{-1} , and the identification of such a feature is not clear. It appears that the results are derived mainly from baseline curvature (resulting from the Christiansen effect). For all the iron sulfide minerals in the reference set, the baseline absorbance is near zero from ca. 1300 to 400 cm^{-1} , but from 1300 cm^{-1} to 4000 cm^{-1} it curves upward.

The second method for indicating accuracy is to examine the spectral residuals from the least-squares fits (Figure 2, Table 4). The worst case was the lignite (coal SL), the large misfit at ca. 1380 cm^{-1} being due to the omission from the reference minerals of nitrate, presumably produced in the low-temperature ash by fixation of organic nitrogen (23). The reproducibility of the 28 original spectra (pooled SD) was 0.05 abs, slightly higher than the pooled standard fit error of 0.04 abs (without the lignite). However, the ten original duplicate spectra gave a pooled standard deviation of only 0.03 abs, which is slightly lower than the fit errors for most of those samples. In general, the fit error approached the experimental error in the original data.

The third method for assessing accuracy is to calculate an elemental composition for each LTA's oxidized ash, based on the reference mineral compositions. Reasonably close agreement between the actual and calculated elemental compositions would substantiate (but not prove) the mineral analysis. The standard error of prediction (SEP) for CaO, Fe_2O_3 , SiO_2 and Al_2O_3 (Table 4) ranged from 3.4 to 6.7 wt % for the various coals. The global SEP was 4.8 wt %. By major ash element, the SEP values were 2.8 for CaO, 5.6 for Fe_2O_3 , 4.5 for SiO_2 and 5.8 for Al_2O_3 . SEP values ranged from 0.3 to 5.7 wt % CaO, 2.3 to 10.3 wt % Fe_2O_3 , 0.1 to 11.6 wt % SiO_2 and 3.0 to 5.6 wt % Al_2O_3 . Inspection of the elemental results also show some bias. CaO values were usually low, Fe_2O_3 values were usually high, and Al_2O_3 values were always low. Calcite impurities may be present in some of the reference spectra, or something else may interfere with the calcite. The high Fe_2O_3 values, even though the pyrite values appear good, indicate that the determined iron oxides, sulfates, and/or siderite concentrations are too high. Somehow, certain iron minerals seem to be replacing or suppressing the appropriate aluminosilicates in the analysis.

In the next section, the potential for factor analysis and related chemometric techniques for providing improvements in the determination of minerals in coal by FTIR are explored.

RESULTS USING PRINCIPAL COMPONENT REGRESSION (PCR)

PCR is a technique in which principal component analysis (one form of factor analysis) of the spectra is followed by regression of the factor scores to calibrate and predict an independently-measured quantity. Besides the spectral

data, these calculations require other data. An accurate mineral analysis of each sample could be used to obtain a calibration. Because this is not possible, one is limited to modeling and predicting other measurable properties such as ash combustion behavior. It is possible to by-pass the mineralogy altogether, and model the desired properties or behavior directly from the LTA spectra. Ash property data which are readily accessible are ASTM ash fusion temperatures (reducing and oxidizing conditions) and ash elemental composition. PLS and PCR are linear models, but are capable of modeling some non-linearities (5). Ash elemental concentrations should be linearly related to intensities of bands in the infrared spectra (under ideal circumstances). Thus, PLS and PCR are expected to do a good job in modeling ash composition. However, ash fusion temperatures are not expected to be linearly related to spectral features.

Infrared data in the 1575-400 cm^{-1} region (1218 points/spectrum) from LTAs from 50 coals (large data set) were used as input data to both PLS and PCR routines. This is the same spectral region used in the classical least-squares analysis of the small data set. Calibrations were developed for the eight ASTM ash fusion temperatures and the four major ash elements as oxides. The program uses PLS1 models, in which only one variable at a time is modeled. Cross-validation was used to select the optimum number of factors in the model. In this technique, a subset of the data (in this case five spectra) is omitted from the calibration, but predictions are made for it. The sum-of-squares residuals are computed from those samples left out. A new subset is then omitted, the first set is included in the new calibration, and additional residual errors are tallied. This process is repeated until predictions have been made and the errors summed for all 50 samples (in this case, 10 calibrations are made). This entire set of calculations is repeated once each time an additional factor is included in the model. The optimum number of factors is near the point at which the residual error reaches a minimum.

Results from these preliminary modeling efforts with the large data set are shown in Table 5. These results were obtained with centering (x and y) and scaling (x) as a data pretreatment. Only PCR results are shown, even though the PLS calculations took less computing time and gave slightly better results. The PCR model is preferred because it provides some additional information on our original data set. Results are depicted graphically in Figures 3 and 4 for the best and worst calibrations, respectively. The main measure of the success of these models is the SEP. For ash fusion temperatures, the SEPs were in the range of 50 to 78°F. The fusion temperatures at oxidizing conditions generally gave slightly better results than those at reducing conditions. These values represent errors somewhat larger than ASTM repeatability and reproducibility limits. The largest single prediction error for these models was about 200°F. This is no larger than the spread in interlaboratory results seen in round robin analyses of standard samples. Furthermore, these results appear to be equivalent to the best predictions of ash fusion temperatures available from ash elemental compositions (24,25,26). Many of those models have incorporated ratios, squared terms and log terms to get better results. It appears that the PLS and PCR models work reasonably well for modeling non-linearities in this case.

The PCR results for CaO , Fe_2O_3 , SiO_2 and Al_2O_3 are quite good, as anticipated. The SEPs for CaO and Fe_2O_3 of 1.7-1.8 wt % are higher than the ASTM reproducibility limits, but the results for SiO_2 and Al_2O_3 are within the ASTM limits for those elements. Note that all these errors are better than the value of 4.8

resulting from the mineralogical analysis. (However, the mineral analysis was not optimized to predict ash elementals.)

The calibrations obtained are valid over a significant range of each property. It is feasible to predict all these properties from the LTA from a small sample of coal, should that be desired. These results mainly show that the methods employed can model other ash properties which are more closely related to large-scale combustion behavior. This is one area where further study is desirable.

Although the software used was not a full-featured factor analysis program, portions of the printed output are useful in studying the spectral data set. The table below shows some information obtainable from PCR models (large data set) with 5, 10 and 13 factors. In this case, the "factors" are principal components derived entirely from the sample data set. PLS factors are not interpretable in the same manner.

<u>No. of Factors</u>	<u>Prediction Residual Sum of Squares (Reconstruction of Original Data)</u>	<u>% of Total Spectral Variance of Data Set</u>
5	89.9	93.5
10	28.1	98.0
13	11.5	99.2

An increase from 5 to 10 in the number of factors representing the original data results in a substantial reduction in the error. Because of the data pretreatment used, the spectral error cannot be directly compared to the experimental error determined from the data set. When five factors were used, two different lignite samples were flagged as possible outliers based on their spectral variances relative to the rest of the data set. With ten factors, one of the lignites was accommodated within the factor model (although ten factors may not have been required to accommodate it). With thirteen factors, both lignites were accommodated.

CONCLUSIONS

Experience in this laboratory has shown that even with careful attention to detail, determination of coal mineralogy by classical least-squares analysis of FTIR data may have several limitations. Factor analysis and related techniques have the potential to remove or lessen some of these limitations. Calibration models based on partial least-squares or principal component regression may allow prediction of useful properties or empirical behavior directly from FTIR spectra of low-temperature ashes. Wider application of these techniques to coal mineralogical studies is recommended.

REFERENCES

1. Given, P. H. and Yarzab, R. F., in Analytical Methods for Coal and Coal Products, C. Karr, Ed. (Academic Press, New York, 1978), Vol. II, p. 3.
2. Robbins, G. A. and Burke, F. P., Proc. 1st Annual Pittsburgh Coal Conference, Sept. 17-21, 1984, Pittsburgh, PA, p. 819.
3. Painter, P. C., Rimmer, S. M., Snyder, R. W. and Davis, A., Appl. Spectro., 35, 102 (1981).

REFERENCES (Continued)

4. Brown, J. M. and Elliott, J. J., "The Quantitative Analysis of Minerals by Fourier Transform Infrared (FT-IR) Spectroscopy", from Workshop on Application of IR Methods to the Study of Clay Minerals, Clay Mineral Society, 20th Annual Meeting, October 1, 1983, Buffalo, NY.
5. Haaland, D. M. and Thomas, E. V., *Anal. Chem.*, 60, 1193 (1988).
6. Renton, J. J., *ACS Fuel Chemistry Div. Prepr.*, 29(4), 21 (1984).
7. Finkelman, R. B., Fiene, F. D., Miller, R. N. and Simon, F. O., Eds., "Interlaboratory Comparison of Mineral Constituents in a Sample from the Herrin (No. 6) Coal Bed from Illinois", U.S. Geological Survey Circular 932 (1984).
8. Davis, D. B., Johnson, L. R. and Mebrahtu, T., U.S. DOE Report DOE/PC/70793--T5, February 1986.
9. Estep, P. A., Kovatch, J. J. and Karr, C., Jr., *Anal. Chem.*, 40, 358 (1968).
10. Tuddenham, W. M. and Lyon, R. J. P., *Anal. Chem.*, 32, 1630 (1960).
11. Stephens, J. D. and Tuddenham, W. M., *Am. Lab.*, 3, 8 (1971).
12. Platbrood, G. and Barten, H., *Anal. Chem.*, 57, 2504 (1985).
13. Huggins, F. E., Huffman, G. P. and Lee, R. J., in *Coal and Coal Products: Analytical Characterization Techniques*, ACS Symposium Series, 205, 239 (1982).
14. Straszheim, W. E. and Markuszewski, R., *ACS Fuel Chemistry Div. Prepr.*, 30(1), 47 (1985).
15. Kalmanovitch, D. P., Montgomery, G. G. and Steadman, E. N., ASME Paper No. 87-JPGC-FACT-4, 1987.
16. Fowkes, W. W., in *Analytical Methods for Coal and Coal Products*, C. Karr, Ed. (Academic Press, NY, 1978), Vol. II, p. 293.
17. Allen, R. M. and VanderSande, J. B., *Fuel*, 63, 24 (1984).
18. Finkelman, R. B., *Scanning Microsc.*, 2, 97 (1988).
19. Zussman, J., Ed., *Physical Methods in Determinative Mineralogy*, Academic Press, New York (1967).
20. Warne, S. St. J., in *Analytical Methods for Coal and Coal Products*, C. Karr, Ed., (Academic Press, NY, 1979), Vol. III, p. 447.
21. Wangen, L. E., Peterson, E. J., Hutchinson, W. B. and Levinson, L. S., in *Environmental Applications of Chemometrics*, ACS Symposium Series, 53 (1985).
22. Harville, D. G. and Freeman, D. L., SPE Paper No. 18120 (1988), and phone conversations with the authors.
23. Painter, P. C., Youtcheff, J. and Given, P. H., *Fuel*, 59, 523 (1980).
24. Gray, V. R., *Fuel*, 66, 1230 (1987).
25. Slegeir, W. A., Singletary, J. H. and Kohut, J. F., *J. Coal Qual*, 7, 48 (1988).
26. Winegartner, E. C. and Rhodes, B. T., *J. Eng. Power*, 395 (1975).

TABLE 1
DESCRIPTION OF COALS

Coals	Rank	Seam - Description
P1	hvAb	Pittsburgh - Underground, Clean Coal, Greene Co., PA
EH	hvAb	Elkhorn 3 - Underground, Unwashed, Breathitt Co., KY
I1	hvBb	Illinois 5,6 - Surface, Clean Coal, Jackson Co., IL
SL	Lig	Scranton - Surface, Mercer Co., ND
I2	hvBb	Illinois 6 - Underground, Clean Coal, Jefferson Co., IL
I3	hvBb	Illinois 6 - Surface, Clean Coal Perry Co., IL
P2	hvAb	Pittsburgh - Underground, Clean Coal, Marshall Co., WV
P3	hvAb	Pittsburgh - Underground, Clean Coal, Monongalia Co., WV
GE	hvAb	No. 2 Gas, Upper and Middle Eagle - Underground, Clean Coal, Raleigh Co., WV
PO	Ivb	Pocahontas 3 - Underground, Clean Coal, Buchanan Co., VA

TABLE 2
REFERENCE MINERALS

MAIN CLASSES

Kaolin - Kaolinite 4, 5, 6, Dickite 16, 27
Mica - Biotite, Phlogopite, Muscovite
Illite - Illite 36, Illite-Bearing Shale
Mixed-Layer Clays - Metabentonite 37, 42
Montmorillonite - 21, 22A, 22B, 24, 25, 26, 31
Felspars - Albite, Anorthite, Orthoclase
Chlorite - Chlorite
Misc. AlSi - Attapulgite, Halloysite, Pyrophyllite 48
Quartz - Quartz, Agate
Fe sulfides - Marcasite, Commercial Pyrite, Mineral Pyrite, Pyhrotite
Fe oxides - Goethite, Hematite, Magnetite
Fe sulfate - Difference spectrum weathered minus unweathered pyrite
Siderite - Siderite
Calcite - Calcite, Aragonite
Gypsum - Gypsum, Drierite
Dolomite - Dolomite

GROUPED CLASSES

Clays - Kaolin, Illite, M. L. Clays, Montmorillonite, Misc. AlSi
Other AlSi - Mica, Feldspar, Chlorite, Quartz
Sulfate - Fe Sulfate, Gypsum
Carbonate - Calcite, Siderite, Dolomite
Fe Altered - Oxides, Sulfate

In addition to spectra of the 42 minerals shown above, the least-squares components included 3 "spectra" representing 1) moisture in KBr blank (obtained by subtraction of 2 KBr blank spectra), 2) a constant baseline offset (1 abs from 4000 to 400 cm^{-1}), and 3) a sloping linear baseline (line from 1 abs at 4000 cm^{-1} to 0 abs at 400 cm^{-1}). Normalization of results used only the 42 mineral components, and disregarded these three components.

TABLE 3

FTIR MINERALOGICAL RESULTS

Mineral Class	P1 (a)		EH (a)		I1 (a)		SL (a)		I2		I3		P2		P3		GE		PO			
	Min.	Max.	Min.	Max.	Min.	Max.	Min.	Max.	Min.	Max.	Min.	Max.	Min.	Max.	Min.	Max.	Min.	Max.	Min.	Max.		
Kaolin	25.8	33.9	11.8	16.6	15.1	21.8	1.1	2.9	23.2	25.2	13.3	14.0	17.6	18.6	20.7	21.2	35.3	35.8	21.6	22.5		
Mica	2.6	6.4	2.9	9.3	0.0	3.3	0.0	-	7.6	10.5	6.1	6.7	5.3	5.5	3.6	4.3	12.1	13.1	4.7	7.7		
Illite	7.1	13.6	20.2	33.8	3.7	47.4	0.0	1.2**	20.8	25.1	9.4	10.8	5.3	5.5	10.0	10.4	8.0	9.9	16.6	17.0		
Mixed Layer																						
Clays	0.0	11.3*	6.2	16.6	0.0	15.8	0.0	-	0.0	-	0.0	-	0.0	-	0.0	-	0.0	-	0.0	-		
Montmorillonite	4.2	13.4	3.4	5.9	0.0	26.0	15.5	20.4	5.0	9.4	13.5	13.8	11.7	11.8	4.9	5.9	4.9	5.9	3.1	3.8		
Feldspar	0.0	3.8	0.0	1.3	0.0	-	0.0	13.5**	0.0	0.7	3.2	3.8	1.6	2.0	9.7	10.1	2.5	2.7	5.4	6.5		
Chlorite	0.6	2.5	3.4	4.9	0.0	2.3	0.0	-	0.0	0.2	0.0	-	0.0	-	2.1	2.5	3.6	3.9	5.0	5.5		
Misc. Clays	1.8	9.8	0.2	2.3	0.0	4.3**	0.0	2.7*	1.7	3.0	0.0	-	2.8	3.3	2.8	3.8	4.0	5.2	0.4	0.6		
Quartz	7.7	13.8	12.5	13.6	11.0	14.6	15.5	20.9	14.1	14.8	14.2	14.2	8.1	8.1	4.9	6.0	12.2	12.9	6.5	7.1		
Fe Sulfide	9.2	13.2	2.0	5.6	0.0	5.3	4.8	13.1	8.0	8.2	19.4	19.6	28.0	29.0	20.8	22.3	4.0	5.1	4.4	7.6		
Fe Oxide	4.7	8.7	5.3	9.2	6.8	8.5	0.0	0.3*	5.5	7.3	4.9	5.6	2.9	3.0	4.8	5.7	7.7	8.3	8.8	10.4		
Fe Sulfate	4.4	11.2	2.9	3.8	0.0	4.5	0.0	-	4.3	5.2	9.0	9.3	14.8	14.9	10.8	11.1	1.0	1.8	0.1	0.5		
Siderite	0.0	-	1.5	2.4	0.0	-	2.4	5.8	0.0	-	3.7	4.0	0.0	-	0.6	1.1	0.0	-	6.3	6.6		
Calcite	0.0	-	0.0	0.0	-	0.0	2.8*	0.0	-	0.0	-	0.0	1.6	0.0	-	0.0	-	0.0	-	9.0	9.4	
Gypsum	0.0	-	0.0	0.5*	0.0	2.3**	34.4	49.2	0.0	-	0.0	-	0.0	-	0.0	-	0.0	-	0.0	-	1.1	1.6
Dolomite	0.0	-	0.0	0.0	-	0.0	-	0.0	-	0.0	-	0.0	-	0.0	-	0.0	0.1	0.0	-	0.0	0.3	

Alternate Classes

Clays	54.0	60.0	55.3	59.7	67.7	71.5	19.6	24.9	56.4	57.0	36.9	37.9	37.7	38.9	39.4	40.4	53.7	55.4	42.8	42.9
Other Alumino																				
Silicates	14.6	22.1	20.5	27.1	13.3	17.2	19.5	34.4	23.2	24.8	24.0	24.1	15.3	15.5	20.9	22.1	30.6	32.5	23.1	25.3
Sulfates	4.4	11.2	3.2	3.8	2.3	5.0	34.4	49.2	4.3	5.2	9.0	9.3	14.8	14.9	10.8	11.1	1.0	1.8	1.6	1.7
Carbonates	0.0	-	1.5	2.4	0.0	2.8*	2.4	5.8	0.0	-	4.0	5.3	0.0	-	0.7	1.1	0.0	-	15.5	16.0
Fe-Altered	9.3	20.0	8.2	12.4	7.5	13.0	0.0	0.3*	10.7	11.6	14.2	14.6	17.8	17.8	15.6	16.8	8.7	10.1	9.3	10.5

(a) Four samples run from each of these coals, two samples run from each of the remaining coals.

*One out of four samples gave a non-zero concentration.

**Two out of four samples gave a non-zero concentration.

TABLE 4
SPECTRAL FIT ERRORS AND ELEMENTAL PREDICTION ERRORS
FROM FTIR MINERALOGY

Coal	Spectral Fit Error (1575-400 cm ⁻¹), Std. Dev. in abs.				SEP Oxide wt % of Ash
	Run 1	Run 2	Run 3	Run 4	
P1	0.028	0.027	0.038	0.041	4.4
EH	0.030	0.033	0.023	0.029	4.3
I1	0.026	0.026	0.029	0.031	4.7
SL	-	0.250	0.149	0.194	4.1
I2	0.033	0.028			5.2
I3	0.037	0.039			6.7
P2	0.040	0.040			4.4
P3	0.037	0.036			5.5
GE	0.038	0.037			3.4
PO	0.022	0.021			6.2

With SL, pooled std. dev. = 0.093

Without SL, pooled std. dev. = 0.041

TABLE 5
PRINCIPAL COMPONENT REGRESSION CALIBRATIONS
FOR SELECTED ASH PROPERTIES

Type	No. of Factors	SEP	Magnitude of Max. Prediction Error	Range of Input Data	
				Min. Value	Max. Value
<u>Ash Fusion Temperature, °F</u>					
RID	5	72.4	169.9	1918	2757
RST	5	77.9	153.5	1972	2808
RHT	5	65.9	201.8	2092	2958
RFT	5	56.2	157.6	2127	2968
OID	6	50.5	117.6	2115	2808
OST	5	60.4	149.8	2159	2858
OHT	5	54.0	163.8	2197	2881
OFT	2	61.1	148.1	2218	2769
<u>Ash Element as Oxide, wt %</u>					
SiO ₂	10	1.38	2.81	29.15	56.45
Al ₂ O ₃	13	0.74	1.33	9.12	27.34
Fe ₂ O ₃	8	1.79	3.19	4.33	30.17
CaO	3	1.73	6.88	1.07	30.11

//s

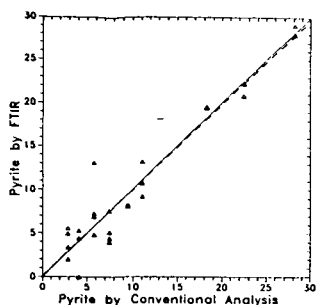


Figure 1. Comparison of FTIR and ASTM Results for Pyrite, wt % of LTA (Solid Line - Parity, Dotted Line - Least-Squares $y = 0.985 x 0.098$)

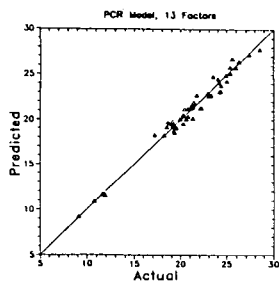


Figure 3. PCR Model Results for Al_2O_3 wt % of Oxidized Ash (Best Model of Ash Properties).

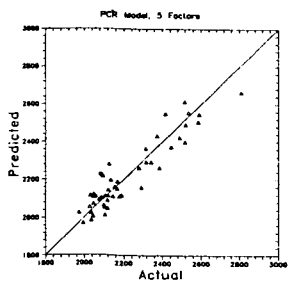


Figure 4. PCR Model Results for Ash Softening Temperature (Reducing), °F (Worst Model of Ash Properties).

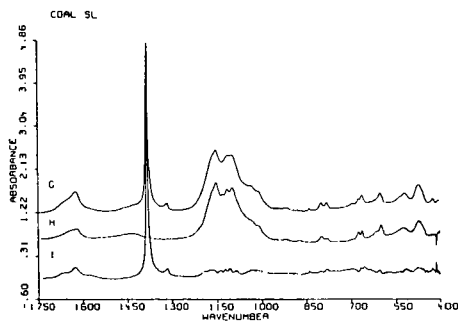
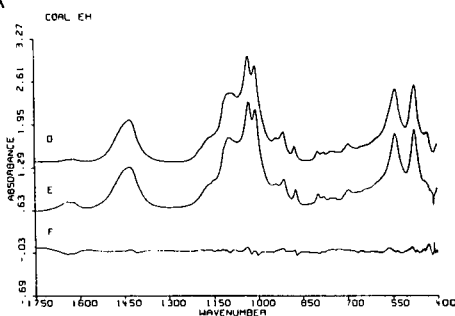
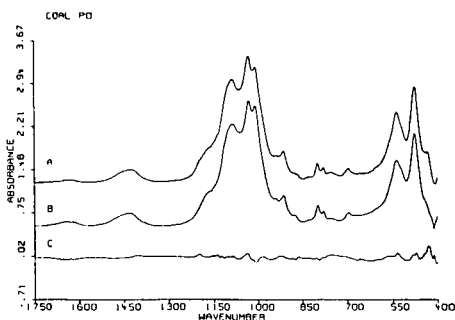


Figure 2. Spectral Residual for the Best (Coal PO), Typical (Coal EH) and Worst (Coal SL) Least-Squares Fits. Spectra Shown are Original LTA (A, D, G), Least-Squares Composite (B, E, H), and Difference (Original Minus Composite C, F, I).